

PHOTOEMISSION SPECTROSCOPY

Fundamental Aspects

Giovanni Stefani

Dipartimento di Fisica "E. Amaldi", Università Roma Tre
CNISM Unità di Ricerca di Roma 3

1. Introduction	2
2. Energy conservation, binding energy and photoelectron energy	3
3. Satellite structures and multiplet splitting	6
4. Chemical shift	10
5. Molecular photoelectron spectra	11
6. Photoelectron angular distributions	17
7. Hole state relaxation	20

1 INTRODUCTION

Photoelectron spectroscopy has been established as one of the most important method to study the electronic structure of molecules, solids and surfaces. It is based upon the photoelectric effect, one of the cornerstones on which quantum mechanic description of matter rests.

In essence, the photoelectron effect amounts to shining a monochromatic electromagnetic radiation ($h\nu$) on a sample and producing free electrons with a well-defined energy spectrum. Einstein equation connects energy of the quantum of the electromagnetic field (photon) with the maximum energy of the ejected free electron (E_e^{MAX}) through a constant characteristic of the sample (work function Φ) $E_e^{MAX} = h\nu - \Phi$. Hence, it establishes a close relationship between sample characteristics and energy spectrum of the ejected electrons and suggests using the photoemission process to build up a wide range of different spectroscopies aimed at studying the electronic structure of matter in its various aggregation states.

Although the photoelectron effect is known since over a century, spectroscopies based upon this phenomenon [1] have developed over the past fifty years, mostly driven by progresses in development of monochromatic, bright and tuneable light sources [2,3].

Now days, photoelectron spectroscopy (PES) has practical applications in many fields of science, such as surface physics and chemistry, material science, nano technologies and still significantly contributes to the understanding of fundamental aspects of physics, chemistry biology etc [4].

The ubiquitous use of photoelectron spectroscopy is testified by the presence of several beamlines devoted to PES in whichever synchrotron radiation source throughout the world.

Aim of the present lectures is to establish the fundamental concepts upon which PES relies in order to turn a photoelectron experiment in a flexible spectroscopic tool to investigate ground state electronic properties of matter. To this end, we shall make use of the quantum description of the interaction between electromagnetic radiation (EM) and matter outlined in Bertoni's lectures [5]. A selected set of experiments on quantum objects as simple as atoms, molecules and clusters, will provide evidences for discussing value and limitations of the approximations needed in order to turn a photionization process into a spectroscopic tool.

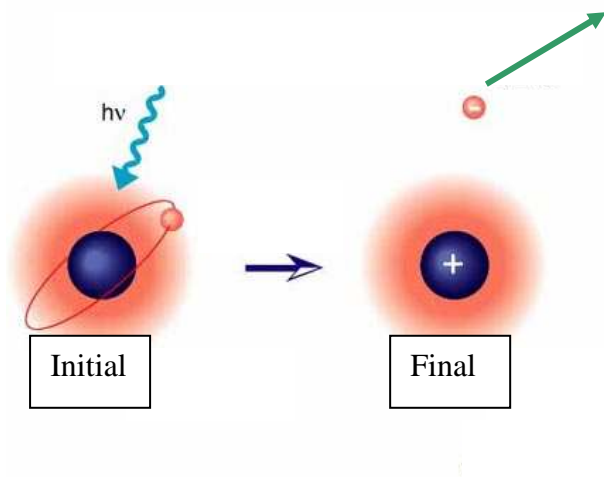


Figure 1. *Schematics of the photionisation process.*

1.1 Basic concepts

The schematics of a modern photoionization spectrometer is shown in figure 2. In essence, the experiments amounts to measuring the photoelectron current (J_e) as a function of the electron kinetic energy (E_e), the electron ejection angle (θ, ϕ) and the spin (σ) for each given energy ($h\nu$) and polarization (ϵ) of the incident photons.

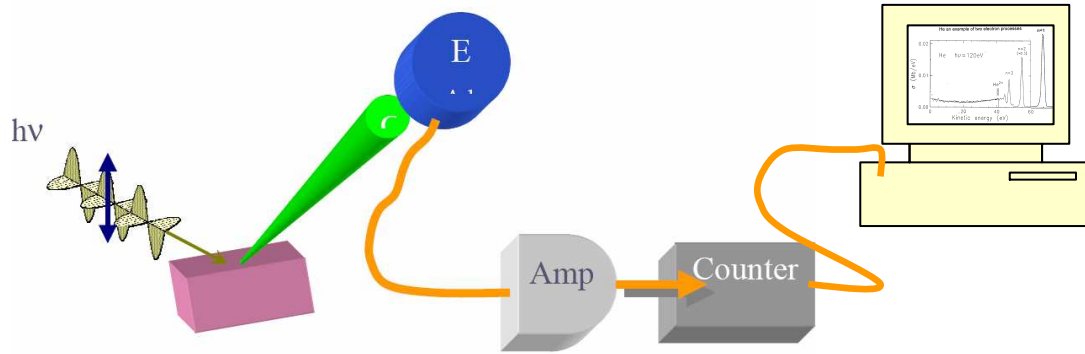


Figure 2 Schematics of a modern photoionization spectrometer. A monochromatic photon beam ($h\nu$) impinges on the sample; photoelectrons emitted within the solid angle Ω defined by the electron detector (E) are energy analysed, detected and properly histogrammed as a function of their kinetic energy.

To this end, it is mandatory to analyse in energy, momentum and (possibly) spin the photoelectrons before detecting them and measuring J_e . This is usually achieved by electrostatic spectrometers in conjunction with electron multipliers that allow for detecting single electrons [6]. The strong interaction of electron with matter imposes to perform experiments under vacuum (at least 10^{-7} mbar) in order to measure a probability distributions of photoelectrons ($J_e(h\nu, E_e, \theta, \phi, \sigma)$) not altered by interaction with the background atmosphere surrounding the sample. As far as photon source is concerned, there are two different types of quasi monochromatic excitation sources that are available under laboratory conditions, namely VUV line spectra of discharge lamps for energies in the range 10-50 eV (UPS), e.g. with rare gases like helium (He Ia=21.23eV and He IIa=40.82eV) and the characteristic lines from the x-ray source (XPS) for which the most commonly used anode materials are aluminium (Al $K\alpha_{1,2}$ =1486,6eV) and magnesium (Mg $K\alpha_{1,2}$ = 1253,6 eV). Although the linewidth is small enough for many applications, i.e. few meV for discharge lamps and slightly below 1eV for x-ray anodes, the use of an additional monochromator can be advantageous for the energy resolution and, more importantly, for suppression of background and satellite intensities. More recently, SR sources have allowed for enhancement of several orders of magnitude in resolution, tenability, wavelength span and polarization control in the x-ray sources (see for instance Margaritondo's lectures at this school) [3].
 Lets' now start to discuss informations obtained by PES.

2. ENERGY CONSERVATION, BINDING ENERGY AND PHOTOELECTRON ENERGY

For sake of simplicity, let's take the simplest many electron quantum system we can find in nature: i.e. the He atom. In such an atom two electrons are bound to a doubly charged nucleus in a $n=1$ $l=0$ $m=0$ $s=\pm 1/2$ quantum state $1s^2$ whose spectroscopic notation is 1S_0 .

According to treatment of EM interaction with matter [5] and within validity of the dipole approximation, a photon is adsorbed by the He atom if the following equation (eq. (41) of [5]) is satisfied

$$\frac{d\sigma}{dh\nu} = 4\pi^2 \alpha h\nu \sum_B \left| \hat{\epsilon} \cdot \left\langle \Psi_B \left| \sum_i \vec{r}_i \right| \Psi_A \right\rangle \right|^2 \delta(E_B - E_A - h\nu) \quad (1)$$

where Ψ_A is the initial state and Ψ_B the final state of the system. To achieve photoionization of He, one of the two electrons must be promoted to the continuum ($E_e > 0$ with respect to vacuum level), see figure 3. Hence, in an experiment where a monochromatic photon is larger than the threshold energy (i.e. the minimum energy needed to ionise the system, see fig.3) is absorbed by an He atom,

the energy conservation δ of equation (1) suggests that electrons are generated with a kinetic energy that satisfies the relation

$$E_B = E_A + h\nu. \quad (2)$$

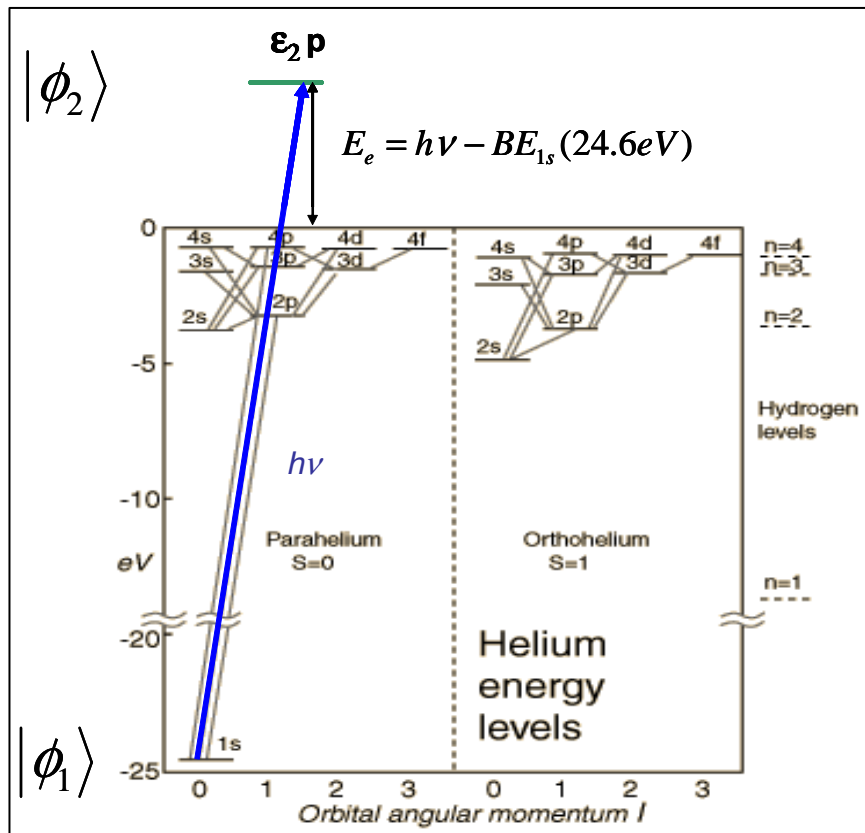


Fig. 3 Diagram of the energy levels of the He atom, the blue arrow represents the photon energy required for the photo ionisation process to take place ($h\nu$), $|\phi_1\rangle$ and $|\phi_2\rangle$ are the single electron initial and final states.

Let's now assume that initial and final states are correctly described in terms of fully independent particles: i.e. $\Psi_A = \hat{A}\phi_1\phi_2$ and $\Psi_B = \hat{A}\phi_1\varepsilon_2$. Under these conditions equation 2 applied to the case sketched in fig 3 reads

$$\begin{aligned} E_{1s} + E_e &= E_{1s} + E_{1s} + h\nu \\ E_e &= E_{1s} + h\nu \\ E_e &= h\nu - BE_{1s} (24.6eV) \end{aligned} \quad (3)$$

Hence, in the Je distribution a single peak is to be expected whose kinetic energy is directly linked to the unperturbed initial state single particle binding energy (BE).

In other words: photoemission spectra should give direct access to spectroscopy of single particle bound states of a multi electron system such as electronic orbitals for atoms, molecules and clusters. A more elaborate concept is needed for photoemission from solids [8].

Is it reality as simple as we think? Let's examine the Je experimental data for Helium (He), the simplest many electron atom. For this atom, the independent particle model is expected to be realistic, and the energy level diagram of figure 3 can be used to represent both initial and final state. In figure 4 is reported the experimental photoemission spectrum of He as measured with a monochromatic photon of 120eV, i.e. the Je(E_e) at a fixed $h\nu$. In case of validity of the fully independent particle model, the observed photoelectron spectrum consists of a single peak, *main*

peak, at the photoelectron energy that satisfies equation 3, the one labelled as $n=1$ at $E_e = 120 - 24.6 = 95.4 \text{ eV}$, that correspond to the transition $h\nu + \text{He}(1s^2) \rightarrow \text{He}^+(1s^1) + \epsilon_{\ell=1}$

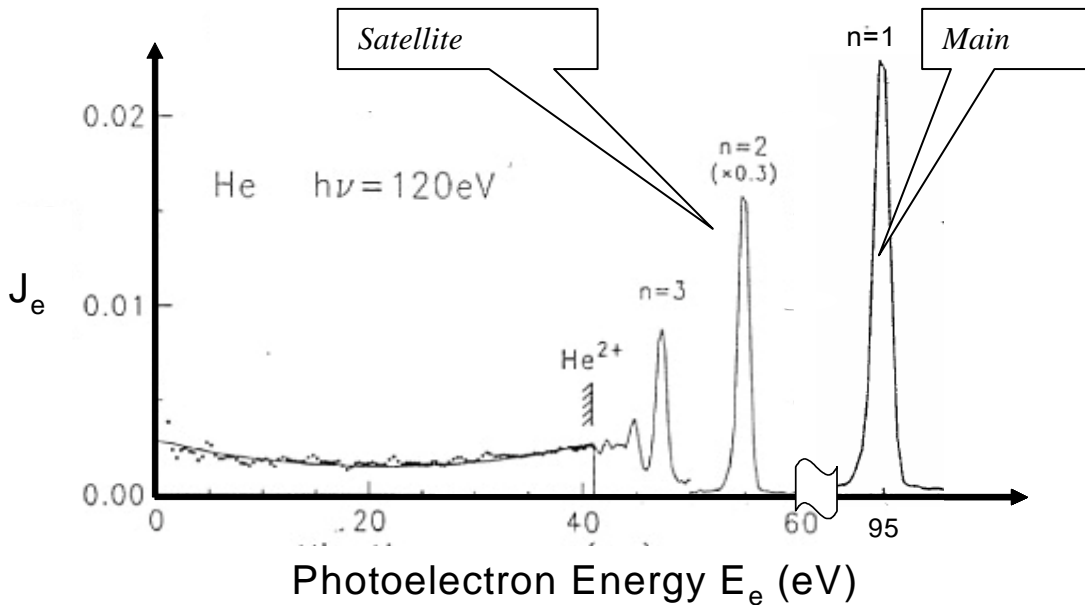
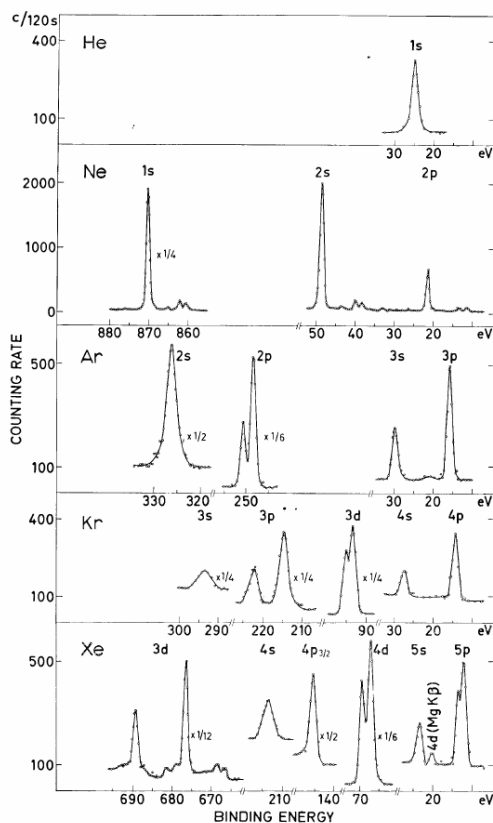


Fig. 4 The He photoemission spectrum as measured at $h\nu=120 \text{ eV}$. The peak labelled $n=1$ correspond to the transition $h\nu + \text{He}(1s^2) \rightarrow \text{He}^+(1s^1) + \epsilon_{\ell=1}$

Further photoemission peaks appearing in the spectrum labelled as $n=2,3,\dots$ and the continuum distribution extending from $E_e=42 \text{ eV}$ to 0 eV , can not be interpreted in terms of independent particle



model and to explain these so called *satellite structures* many-body properties of the systems should be taken into account. Similar *satellite structures* are observed for all the rare gases and, as shown in figure 5, they become more and more relevant as the atomic number increases. This overview of the photoemission spectra, as measured for a photon energy of 1486.6 eV , clearly shows that besides the already mentioned *satellites*, the *main peaks* corresponding to final state with a single hole in orbitals with angular different from 0 (p, d, f, ...) display a doublet structure ascribable to spin-orbit splitting. We shall see in the following that for targets of increased complexity, such as molecules clusters or solids, the photoelectron spectrum is accordingly more complex. To interpret these spectra asks for models more sophisticated than the one outlined in equation 3, and this will be discussed in the following paragraphs.

Figure 5. Rare gases photoemission spectra at $h\nu=1486.6 \text{ eV}$. J_e is plotted as a function of the single particle binding energy $BE_{n,l} = h\nu - E_e$. The label $n\ell$ indicates the ionic single particle hole state.

3. SATELLITE STRUCTURES AND MULTIPLLET SPLITTINGS

To understand the origin of the *satellite features* appearing in the photoemission spectra we shall use as a case study the He Je spectrum. The spectrum is reported in details and for various photon energies in figure 6. Besides the peak associate with the final state $1s^1$ foreseen by the independent particle approach, a manifold of discrete transitions at larger “apparent” BE followed by a continuum, above a certain threshold, is also clearly observed, though with an intensity that is roughly 1/100 the intensity of the main peak.

3.1 Satellite structures

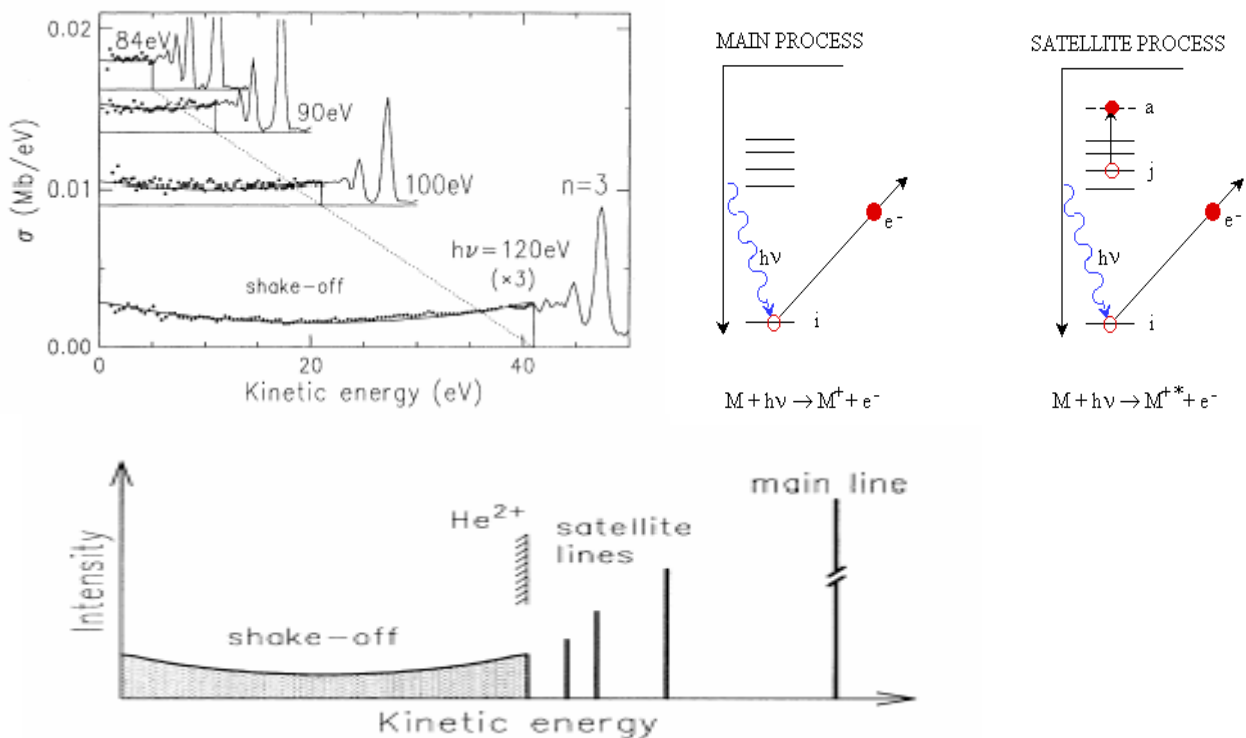


Figure 6 *Experimental He satellites structures in the photoemission spectrum for photon energies ranging from 84 to 120 eV and for final ions excited to the $n=3$, or larger, electronic state. The energy level diagrams are sketches of the mechanism responsible for generation of the main peak (one electron transition) and satellite structures (two electron transitions, see text for details). Diagram to the bottom of the figure represents the expected overall photoemission spectrum.*

In building up the aforementioned energy conservations (eq. 3), we have implicitly assumed validity of the “frozen core approximation”, i.e. relaxation of the sample upon creation of a hole-state and electron electron correlation is neglected. To overcome these limitations the system is to be described as formed by N interacting electrons whose energy eigenvalues are defined according to the Schrodinger equation:

$$H_0 |\Psi_A^{(N)}\rangle = E_A^{(N)} |\Psi_A^{(N)}\rangle \quad (4)$$

Where the initial state Hamiltonian is

$$\begin{aligned}
 H_0 &= H_0(kin) + H_0(e-n) + H_0(e-e) + H_0(s-o) = \\
 &= \sum_1^N \frac{p_i^2}{2m} + \sum_1^N -\frac{Ze^2}{r_i} + \sum_{i>j}^N \frac{e^2}{r_{ij}} + \sum_1^N \zeta(r_j) \vec{l}_i \bullet \vec{s}_i
 \end{aligned} \quad (5)$$

and the N-particle wave function is simply described by a Slater determinant of one electron spin-orbitals for both the initial:

$$\left| \Psi_A^{(N)} \right\rangle = \hat{A}(\phi_j(\vec{r}_i, \sigma_i); \Psi_R^{(N-1)}) \quad (6)$$

and the final state

$$H_0' \left| \Psi_B^{(N)} \right\rangle = E_B^{(N)} \left| \Psi_B^{(N)} \right\rangle \quad (7)$$

of the photoionisation process, where H_0' is the final state Hamiltonian (note that in general H_0 is not equal to H_0').

Assuming validity of the Sudden Approximation: i.e. the electron in the continuum state $|\varepsilon_l\rangle$, with kinetic energy E_e and momentum \vec{K}_e , (photoelectron) is fully decoupled (doesn't interact) from the residual (N-1) particles ion, the final N-particle state can be expressed as

$$\left| \Psi_B^{(N)} \right\rangle = \hat{A}(\varepsilon_l; \left| \Psi_B^{(N-1)} \right\rangle) \quad (8)$$

To appreciate consequences of the many-particle descriptions of the atom on the Je spectrum, let's write down the photoemission cross section at fixed photon energy and differential in the photoelectron energy and emission angle. It derives directly from the absorption cross section (1) that, in the case of a discrete-to-continuum transition, represents the total probability of photoemission over the 4π solid angle.

By replacing expressions (6) and (8) in equation (1) we obtain:

$$\frac{d\sigma}{d\Omega dE_e} \prec \frac{1}{h\nu} \sum_{A,B} \left| \hat{\varepsilon}_l \bullet \langle \varepsilon_l | \vec{r}_j | \phi_j(\vec{r}_j, \sigma_j) \rangle \langle \Psi_B^{(N-1)} | \Psi_R^{(N-1)} \rangle \right|^2 \delta(E_e + E_B^{(N-1)} - E_A - h\nu) \quad (9)$$

In passing we note that the total photoionization cross section is inversely proportional to the photon energy and, in general, has a maximum at threshold. In figure 7, the calculated total photoionization cross section for He and Xe is reported as a function of the photon energy.

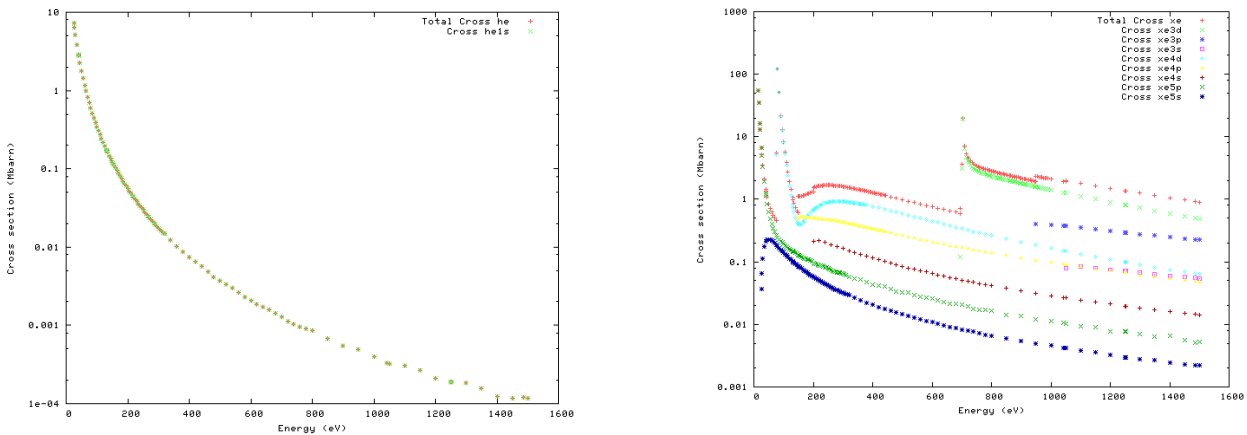


Figure 7. He and Xe total photoionization cross sections as a function of the photon energy

Assuming validity of the Koopman's theorem, i.e. the target atom electronic structure stay frozen under creation of the hole state, Hamiltonians of initial and final states are identical ($H_0=H_0'$) and the monopole matrix element appearing in (9) reduces to a δ function between the final ionic state and the initial (N-1) residual. As a consequence, the photoemission cross section will be different from 0 (Je different from 0) only for the ionic states that correspond to the frozen residues at N-1 of the initial N particles ground state. In this way relaxation and correlations are overlooked, energy conservation reduces to the δ function appearing in (9) and the Koopman's energy of the photoelectron is directly linked to the binding energy of single particle orbital involved in the photoionization process. Under these circumstances, the only allowed photoemission process for He is: $h\nu + He(1s^2) \rightarrow He^+(1s^1) + \varepsilon_{\ell=1}$ that is associate to the most intense peak appearing in figure 4 (Main line or adiabatic peak). To explain the feint structures highlighted in figures 4 and 6, the condition $H_0=H_0'$ must be relaxed, thus allowing for a spectrum of possible final ionic states to be associate with removal of an identical single particle spin orbital. There is a manifold of different final states associate to each individual single particle hole state that imply excitation of further electron(s) of the target both to discrete and continuum empty states (shake-up and shake-off satellites respectively). The monopole matrix element of (9) determines which final states are allowed (monopole selection rules) and with which probability. In the case of He, for instance, the main allowed transitions present in the spectrum are:

$$h\nu + He(1s^2) \rightarrow He^+(1s^1) + \varepsilon_{\ell=1}$$

$$h\nu + He(1s^2) \rightarrow He^+(2s^1) + \varepsilon_{\ell=1}, He^+(3s^1) + \varepsilon_{\ell=1}, He^+(4s^1) + \varepsilon_{\ell=1}, \dots, He^{++} + \varepsilon_{\ell} + \varepsilon_{\ell'}$$

$$h\nu + He(1s^2) \rightarrow He^+(2p^1) + \varepsilon_{\ell=0}, He^+(3p^1) + \varepsilon_{\ell=0}, He^+(4p^1) + \varepsilon_{\ell=0}, \dots, He^{++} + \varepsilon_{\ell} + \varepsilon_{\ell'}$$

These transitions explain most of the satellite structures observed but the next question is: can E_c still be directly connected to single particle binding energies? It can be shown that sum rules applicable to photionization process imply that: i) the weighted average of all binding energies (main, shakeup and shake off) yields the Koopman's Theorem binding energy ($BE_{n\ell m}$), ii) the sum of all intensities is proportional to the frozen orbital cross section ($|\hat{\varepsilon} \cdot \langle \varepsilon_i | \vec{r}_j | \phi_j(\vec{r}_j, \sigma_j) \rangle|^2$).

This kind of treatment is very convenient for atoms, molecules and core states of solids, i.e. for all localized electron states. In the case of valence state of solids, i.e. whenever we are dealing with delocalised, continuum electronic state, it is more convenient to formulate the matrix element $\langle \varepsilon_i | \vec{r}_j | \phi_j(\vec{r}_j, \sigma_j) \rangle \langle \Psi_B^{(N-1)} | \Psi_R^{(N-1)} \rangle$ of (9) as $\langle \varepsilon_i | \vec{r}_j | \phi_j(\vec{r}_j, \sigma_j) \rangle A(\vec{k}, E)$ where $A(\vec{k}, E)$ is the so called spectral function of the target that can be related to the single particle Green's function. In spite of the formal differences, the conclusions that we have reached on the meaning of main ad satellite lines of a photoelectron spectrum are valid independently of the state of aggregation of the target. In particular, the richness of satellite structures is directly linked to the degree of electron correlation that affects the initial bound state involved in the photoionization.

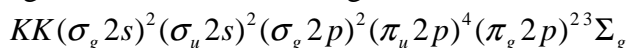
3.2 Spin-orbit splitting

An inspection of the photoelectron spectra reported in figure 5 shows that besides the aforementioned satellite structures, further splitting of the photemission peak associate with $\ell \neq 0$ hole states is noticeable. This is particularly evident in the case of the Xe 3d doublet. This is a typical final state effect. In these closed shell atoms the initial state energy doesn't depend upon spin momentum projections as all orbitals are fully occupied. On the contrary, when a vacancy is created in the orbital identified by n, l, m quantum numbers, the energy of the final state depend on the spin projection through the term $H_0(s-o)$ of the Hamiltonian (5). Hence, it is to be expected that

holes in p ($l=1$) and d ($l=2$) will generate doublets of final states characterized by quantum number j ($j=1+s$) equal to $1/2$, $3/2$ and $3/2$, $5/2$ respectively.

3.3 Multiplet splitting

In moving from closed to open shell systems (i.e. quantum system in whose orbitals are partially occupied) complexity of the photoelectron spectrum increases and splitting of peaks not ascribable to spin-orbit interaction is observed. Such effects, usually termed as “multiplet splitting”, were firstly observed in connection with core photoemission from paramagnetic free molecules and transition metal compounds. An introductory example of multiplet splitting as observed in the photoemission spectra from core O 1s electrons in the paramagnetic free molecules O₂ is given in figure 8. The electron configuration of the neutral ground state is:



As shown in the figure 8, ionization of the K shells leads to two different core hole multiplet states of O₂⁺, one with ²Σ_g⁻ - symmetry, the other of ⁴Σ_g⁻ - symmetry. Figure 8 also shows the XPS spectrum with two separate lines corresponding to these two different final electronic states.

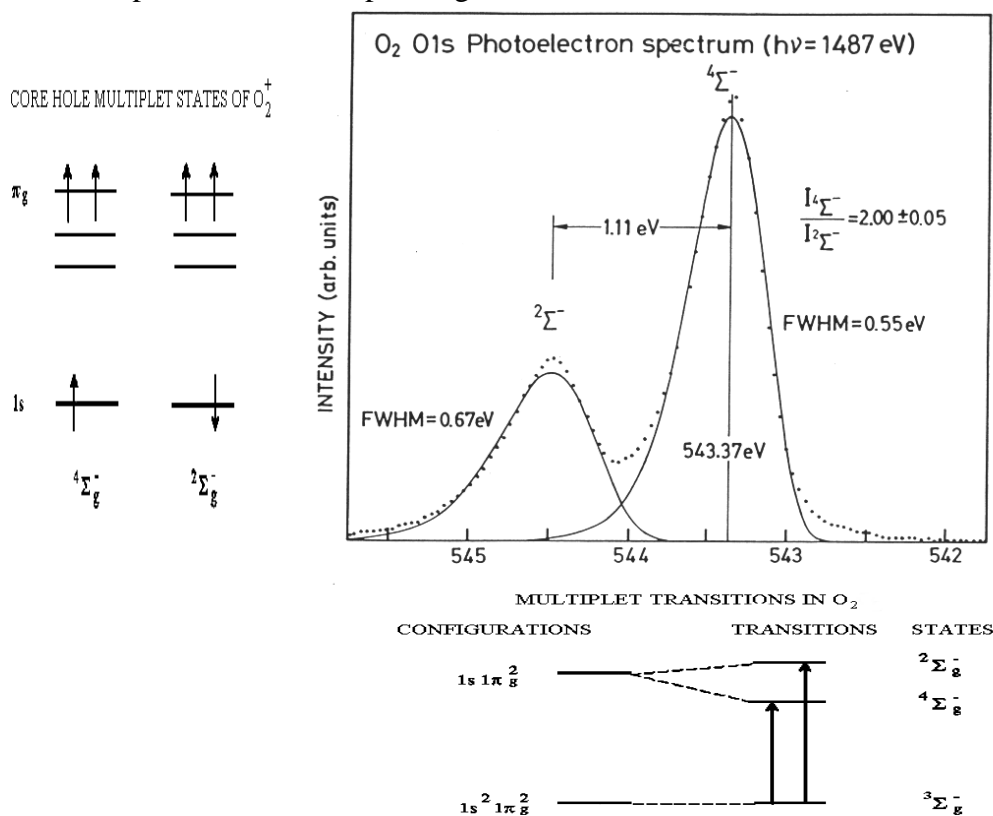


Figure 8. O 1s core photoemission spectrum of molecular oxygen as measured with 1487eV photons. The observed multiplet splitting of 1.11eV correspond to the two possible final states outlined in the left side schematics. Energetic of the initial, neutral, and two final ionic states is also shown.

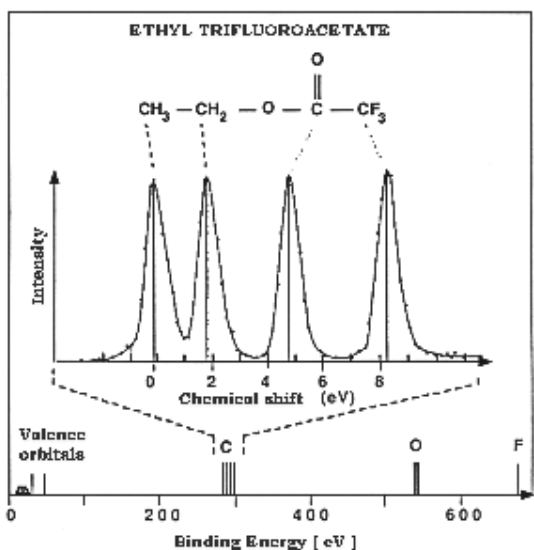
The transitions observed in the photoelectron spectrum can be schematically illustrated as shown in the diagram at the bottom of the figure. The difference in transition energy towards the two different final states, 1.11eV, arise from spin coupling of the residual 1s core electron with the valence electrons unpaired spins. Relative weight of the two peaks obeys the statistical ratio expected for quartet versus doublet intensity, i.e. 2.

It is worth noting that multiplet splittings are observed for both core and valence photoelectron spectra. The valence spectrum of the oxygen molecule, for example, shows very well separated

doublet and quartet states (we shall see this in paragraph devoted to molecular spectra). It may also be noted that multiplet splittings are common ingredients in core hole relaxation processes, such as Auger electron spectra, since the final states normally contain two vacancies which may couple in several different ways and give rise to states of different energy.

4. CHEMICAL SHIFT

It is well known that when aggregating atoms to form molecules, clusters or solids, the valence



electrons are mostly involved to form bonds while core state remain almost unchanged in their atomic character (negligible overlap between adjacent atoms core orbitals). Nevertheless, a considerable fraction of photoelectron studies has been primarily involved with the precise measurement of core hole electron binding energies and in particular of what is known as the “chemical shift” suffered by these energies when the chemical environment within which the atom is bound changes. Let’s exemplify this effect with an experimental example. In figure 9 is shown the photoelectron spectrum of the Ethyl-trifluoroacetate molecule. In this organic molecule are present 4 carbon atoms in four different local chemical environments.

Figure 9. *C1s* photoelectron spectrum of ethyltrifluoroacetate showing four different lines due to the chemical shift. The spectrum was excited by monochromatized radiation at 1487 eV.

Each individual carbon atom gives rise to a different core photoemission peak, thus allowing for

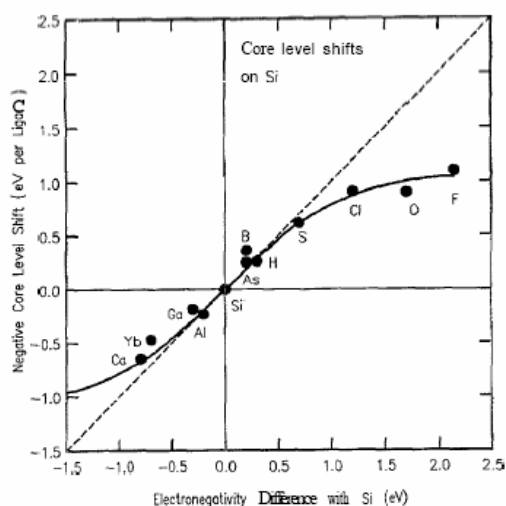
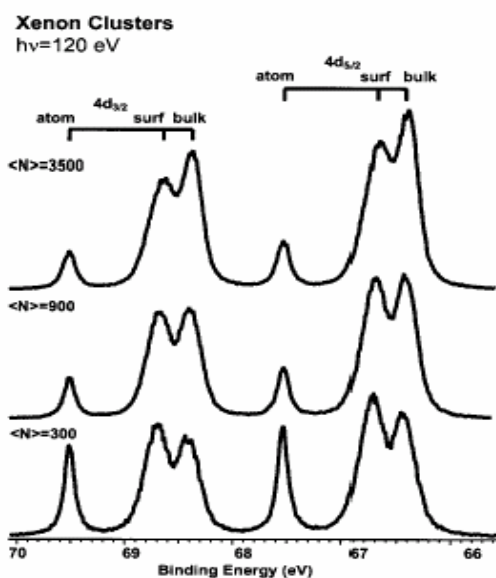


Figure 10. *Silicon 2p* chemical core level shift plotted as a function of the difference in electronegativity between Si and bond partner.

Vice versa, when bound to elements with smaller electronegativity there is more charge available for screening and e-e-interaction and the core binding energy accordingly decreases. The chemical shift provides chemically-significant information concerning the initial state electronic structure of the system under study. Both initial (electronegativity) and final (relaxation of neighbouring

electrons on the hole) states effects are influenced by chemical environment and contribute to determining chemical shift.

Empirically, there seems to be a correlation, although exception exists, between chemical shift and electronegativity of neighbour atoms. For small electronegativity differences $\Delta\chi$ the core level shift ΔE is nearly equal to $\Delta\chi$. At larger $\Delta\chi$ the energy shift saturates, probably due to saturation of the charge transfer. From such an empirical curve, one may predict core level shift for new ligands, or find out from a measured core level shift which ligand (electronegativity of the ligand) is involved. To accurately calculate chemical shifts is to be taken into account the total “all electron energies” with and without core hole. In spite of the complexity of this phenomenon, an overall



proportionality between binding energy and electronegativity is found in most of the cases, as clearly shown by the graph in figure 10 where binding energy of Si 2p orbital as a function of the electronegativity of the bond partner atom is reported.

Core energy shift is also associate to changes in coordination number of the same atom within a given aggregate. Clusters give a clear example where atoms bound to the outermost shell (surface) experience a chemical bond different from those bound to the inner shells (bulk). Figure 11 gives an example of Surface-Bulk shift of core photoemission spectra in rare gases clusters.

Figure 11. *4d photoemission spectra of xenon clusters of three mean size at 120 eV photon energy: $\langle N \rangle = 300, 900, \text{ and } 3500$*

5. MOLECULAR PHOTOELECTRON SPECTRA

The next complex quantum system whose electronic structure is to be investigated by PES is a

molecule. It is evident that the extra degree of freedom added to the system by the nuclear motion (i.e. molecular vibrations and rotations) will play a role in the related photoelectron spectra. In this case, energy can be transferred from the electromagnetic field to electronic, vibrational and rotational degrees of freedom of the quantum system. In other words, we ask ourselves how vibrations and rotations will influence molecular photoelectron spectra. Even though we start from a ground state configuration, vibrational and rotational excitations are to be observed besides the electronic ones.

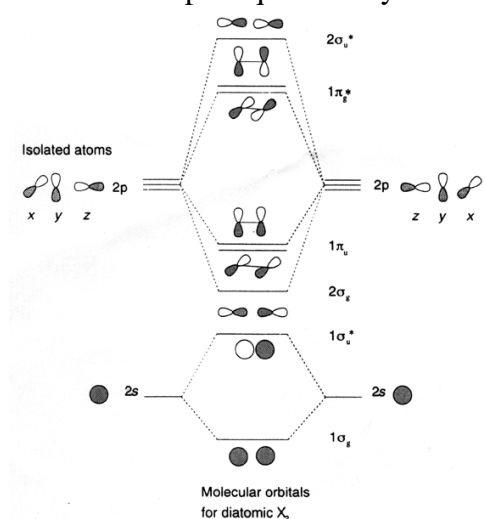


Figure 12. *Molecular orbitals for a diatomic X_2 as built from constituent atomic levels.*

Let's take as an example simple diatomic molecule, the basic principles laid down in this case remain valid for more complex polyatomic molecules though experimental and theoretical treatments will become accordingly more complex. The electronic energy level diagram for a diatomic molecule is depicted in figure 12 with orbitals up to the $1\Pi_u$ occupied (HOMO) and with empty orbitals starting from the $1\Pi_g^*$ (LUMO).

5.1 Vibrational overtones

Nitrogen is an archetypal for diatomic molecules and the expected photoemission spectrum is shown in figure 13 (central panel) as a function of the single-particle binding energy and alongside with the molecular orbital diagram assignments (left most panel). Note that the antibonding orbitals are not labeled as such (no asterisk). The molecule has a center of inversion and this allows us to classify the orbitals as "g" or "u".

Comparison with the experimental PES spectrum (right most panel), note that vertical axis is the binding energy while the horizontal one is the photoelectron current intensity, shows that actually the three outermost occupied orbitals give rise to three distinct multiplets.

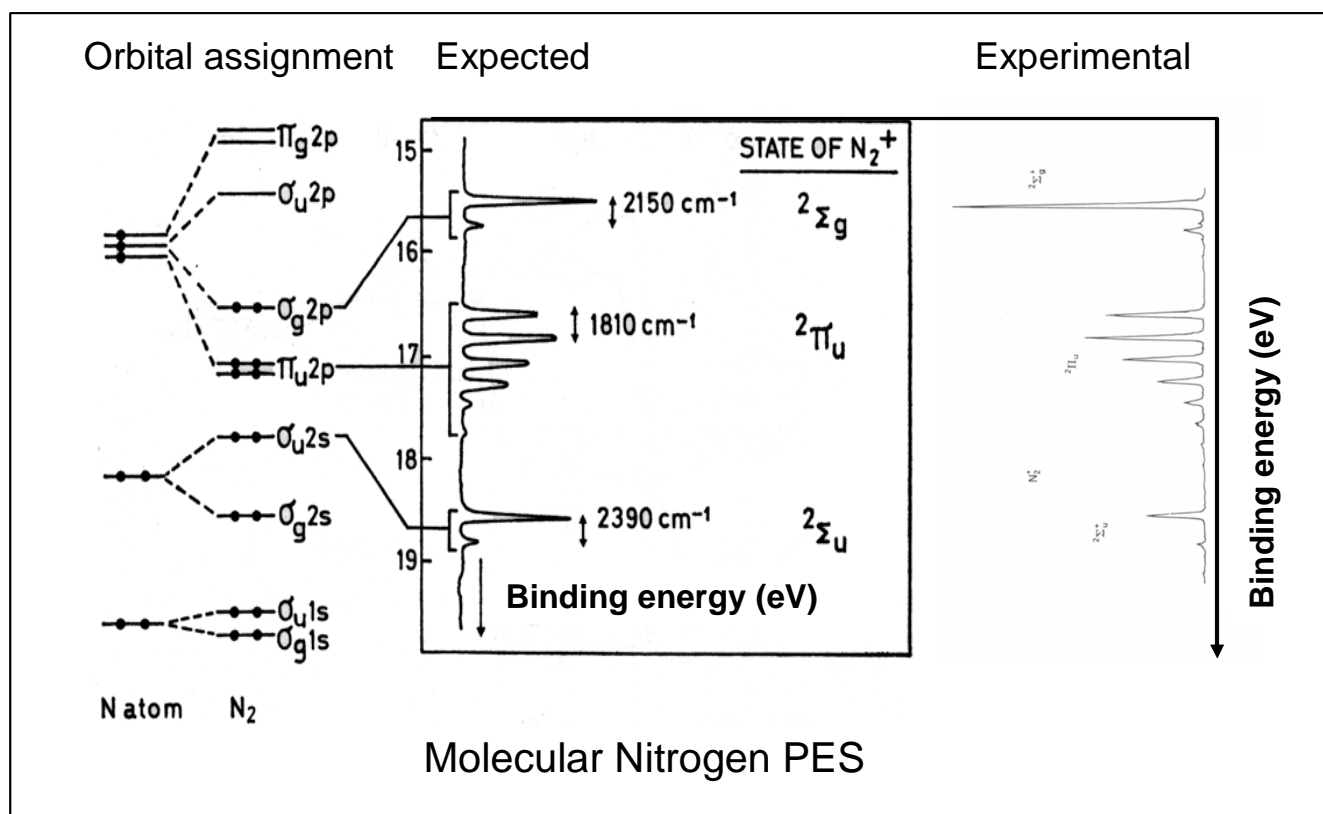
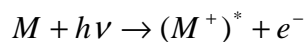
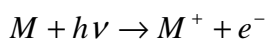


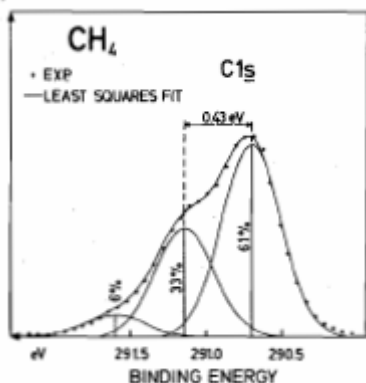
Figure 13 *Molecular PES of N_2 . The central panel displays the expected PES while the right panel shows the experimental one. The molecular orbital diagram assignment is reported in the right panel.*

The existence of a fine structure (side bands) for the individual electron states is ascribable neither to spin-orbit nor to multiplet splitting. The origin of this fine structure is due to an effect that we have neglected so far, namely the generation of the ionized molecule in excited vibrational states. If the electron is ejected and the ion is in an excited state, the excitation energy will be lost for the electron which accordingly has a lower kinetic energy than expected.



The observed magnitude of the energy splitting in the fine structure (e.g. 2390 cm^{-1} for the ${}^2\sigma_u$ band in nitrogen) shows that we are dealing with vibrationally excited states.

Vibrational effects are observed in core photoemission spectra as well, as it is demonstrated by the spectrum appearing in the figure 14. It refers to C 1s photoionisation in CH_4 and



displays two overtone peaks displaced by 0.43 and 0.86 eV, respectively, from the carbon main transition. The observed energy splitting is consistent with the vibrational quantum in $\text{CH}_4(\text{C}1s^{-1})$ while the relative intensities are explained in terms of Frank-Condon [see note 1] factors for transitions to the $v=1$ and $v=2$ ionic excited states. Vibrational excitation of the initial ground state is not taken into account as the sample was at room temperature and the nitrogen vibrational quantum is of the order of 400meV.

Fig 14 *C1s photoemission spectrum in CH_4 . The C1s main line is accompanied by two overtone lines corresponding to formation of the core ionised molecule in the $v=1$ and $v=2$ excited states.*

Vibrational fine structure is usually clearly visible in UPS (typical energy resolution 0.015 eV) but is obscured in XPS (typical energy resolution 1 eV). Note that a resolution of 0.015 eV corresponds to 120 cm^{-1} ($1 \text{ eV} = 8066 \text{ cm}^{-1}$). This is sufficient to observe a vibrational fine structure but not enough to resolve the rotational fine structure.

To explain the main features of the molecular photoemission spectrum we shall calculate the differential photoemission cross section taking into that initial and final single particle electronic states are molecular states. For core states, localization of the electronic state makes atomic like orbitals appropriate for describing both bound and continuum states and atomic like cross section is appropriate.

Situation is more complex for valence delocalised initial states (molecular orbitals) that are described in terms of the usual Born-Oppenheimer approximation, i.e. as the product of linear combinations of atomic orbitals (LCAO) with independent nuclear motion wavefunctions. Initial and final states should take into account the full geometry of the molecular system and the photoelectron continuum state should account for interaction with the residual molecular ion, though at high energy and large distance from nuclei it can be assumed to be an atomic continuum. The simplest approximation to continuum wave functions is the Plane Wave (PW) and several other more elaborate models have been successfully applied (OPW, multiple scattering, etc.).

To calculate the molecular photoemission cross-section we shall follow Gelius approach for XPS where the photoelectron is described as a PW and initial states are described by LCAO. Furthermore, the BO approximation allows factorising the WFs in a product of electronic and vibrational WFs (we neglect rotational states as they are usually not resolved in PES and XPS).

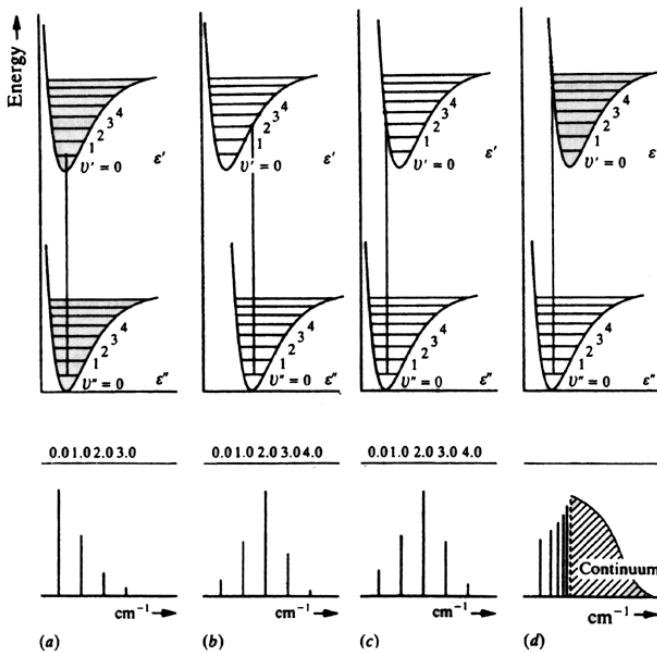
In other words, the system hamiltonian should now include the nucleus-nucleus interaction

$$\begin{aligned}
 H_0 &= H_0(kin) + H_0(e-n) + H_0(e-e) + H_0(s-o) + H_0(s-o) = \\
 &= \sum_1^N \frac{p_i^2}{2m} + \sum_1^N -\frac{Ze^2}{r_i} + \sum_{i>j}^N \frac{e^2}{r_{ij}} + \sum_1^N \zeta(r_j) \vec{l}_i \cdot \vec{s}_i + \sum_{i>j}^M \frac{e^2 Z_i Z_j}{r_{ij}} \quad (10)
 \end{aligned}$$

and the WFs read: $|\Psi_{A,B}^{(N)}\rangle = |\Psi_{A,B}^{(N)el}\rangle |\Psi_{A,B}^{vib}\rangle$. Hence, substituting these initial and final states WFs in the photoemission cross-section (9), we obtain the molecular expression of the photocurrent J_e as calculated under the aforementioned approximations.

$$\frac{d\sigma}{d\Omega dE_e} \propto \frac{1}{h\nu} \sum_{A,B} \left| \hat{\epsilon} \cdot \left\langle \epsilon_l \left| \vec{r}_j \right| \sum_{A\lambda} C_{A\lambda} \phi_{A\lambda} \right\rangle \left\langle \Psi_B^{(N-1)el} \left| \Psi_R^{(N-1)el} \right\rangle \right|^2 \left| \left\langle \Psi_B^{vib} \left| \Psi_A^{vib} \right\rangle \right|^2 \delta(E_e + E_B^{(N-1)} - E_A - h\nu) \quad (11)$$

In the molecular photoelectron spectrum we shall therefore expect as many peaks as many ionic electron-vibrational states are allowed by monopole and vibrational selection rules and with intensities proportional to product of the relevant Frank-Condon and Fractional-Parentage



coefficients. The way FC coefficients will work in a molecular photoionization process is sketched in the figure 15 where the relative probability for exciting final ions in $v=1,2,3,\dots$ states is depicted as a function the molecular equilibrium distance of the final ion. As it gets larger and larger with respect to the ground neutral state equilibrium distance, increasingly higher v states are accessed in the final ion, till the fragmentation threshold is reached and excitation (discrete vibrational structure in the photoemission spectrum) as well fragmentation (continuum vibrational structure in the photoemission spectrum) are present.

Figure 15. Schematics of the dependence of PES features upon change of the molecular equilibrium distance in the final state molecular ion. Minimum change is the leftmost panel, maximum change is the rightmost one.

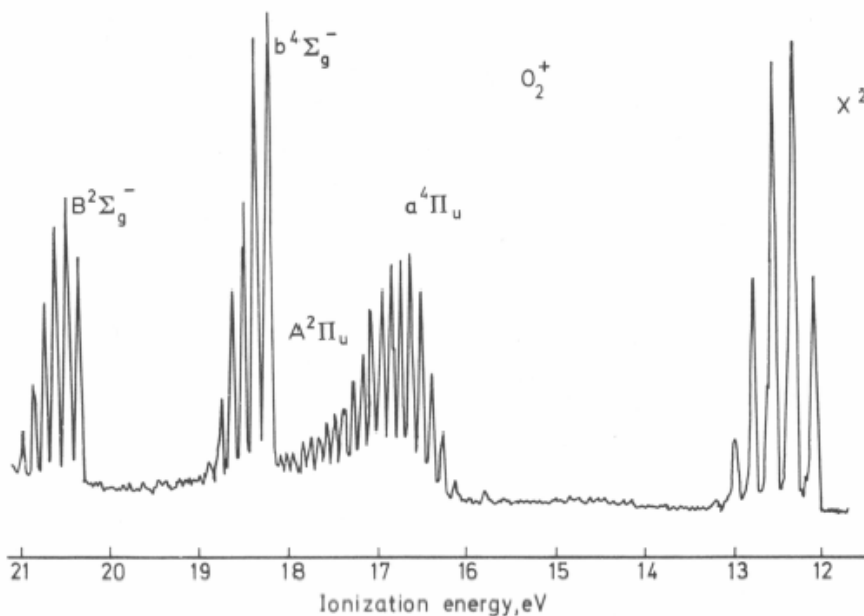
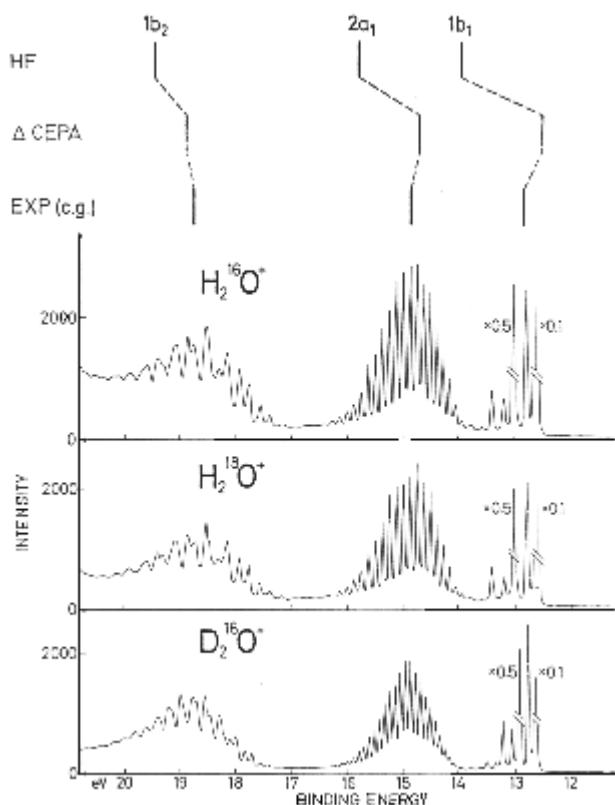


Figure 16. The valence photoelectron spectrum of the oxygen molecule excited by monochromatized HeII radiation at 40.814 eV. Note the multiplet splitting into a doublet and a quartet component for many of the states.

Multiplet splitting is present in molecular spectra as well. A clear example of the experimental vibrational structure observed in the valence photoionization spectrum of molecular oxygen in conjunction with the aforementioned quartet doublet multiplet splitting is given in the PES of O₂, with HeII exciting light, shown in figure 16.



Extensive vibrational structures have been observed also in PES of polyatomic molecules, water is a relevant example. The PES spectrum excited by HeIa radiation at 21.218 eV is shown in figure 17 (top experimental spectrum). Binding energies for the three outermost valence orbitals have been calculated using a one-electron method (HF) and a many-electron (CI) method and are given in the upper part. Comparison of the predicted binding energies with the centre of mass of the vibrational structure associate to each individual orbital highlights the extreme sensitivity of PES to accurateness of the model adopted in describing the molecular valence orbitals .

Fig.17. Gas phase photoelectron spectra of some different isotopic variants of the water molecule excited by HeIa radiation at 21.218 eV. Calculated results using a one-electron method (HF) and a many-electron (CI) method are given in the upper part. The spectra show extensive vibrational structure.

Sensitivity of PES vibrational overtones to nuclear masses is depicted in the spectra of isotope modified water molecules, ¹⁸O instead of ¹⁶O and D instead of H, shown in the two lower panels of figure 17. Modern molecular PES studies include spectroscopy of transient states and species as well, but this subject is well beyond the scope of these lectures.

5.2 The Jahn-Teller splitting.

For polyatomic molecules with a high degree of symmetry orbitals of the ionic state that have identical eigenvalues (degenerate) are possible. For example, the electronic ground state of the ammonia molecule may be written $N1s^2 1a_1^2 2a_1^2 1e^4 (^1A_1)$, that is totally symmetric and non-degenerate. By removing one electron from the e-orbital, the orbitally degenerate doublet state $N1s^2 1a_1^2 2a_1^2 1e^3 (^2E)$ is formed. The Jahn-Teller theorem proves that this state is unstable, and that the equilibrium geometry is found at a lower symmetry, from C_{3v} to C_s , where the same electron configuration may be written as:

$$N1s^2 (1a')^2 (2a')^2 (1a'')^1 (3a')^2 (^2A'') \text{ or } N1s^2 (1a')^2 (2a'')^2 (1a'')^2 (3a')^1 (^2A')$$

In this new symmetry the orbital degeneracy is removed but the states are not well defined as the configurations are mixed by the vibrational motions. Hence, a splitting into two component states may be observed in PES if the ionization involves an orbital which substantially influences the molecular geometry, i.e. a bonding orbital. In fact, the 2E state in the photoelectron spectrum of ammonia shows such a splitting of about 1 eV. Since it is the chemical properties of the orbital that will primarily determine the magnitude of the splitting, Jahn-Teller instabilities are observed mainly in the valence region.

An example of a Jahn-Teller splitting, as well as a spin-orbit splitting, is seen in the spectrum of the methyl bromide (CH_3Br) molecule (see figure 18). The outermost band shows the spin-orbit splitting in the $(2e)^3\ ^2E$ state. This band also shows some vibrational structure. The $2e$ orbital is a non-bonding, C lone-pair orbital and shows therefore no large Jahn-Teller instability. The photoelectron band, observed between 14.5 and 17 eV, shows a Jahn-Teller splitting into two broad components separated by 0.8 eV. Since the symmetry of this state is lowered, the orbital angular momentum is quenched and so is the spin-orbit coupling.

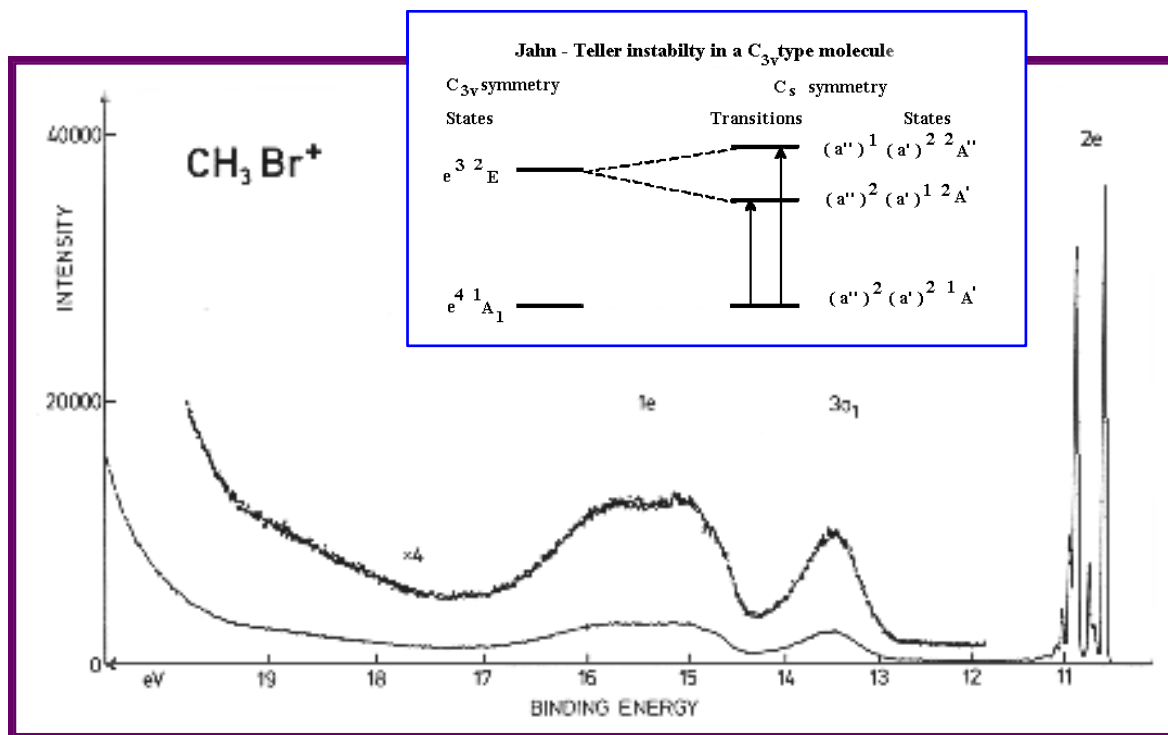


Fig.18 The HeI excited photoelectron spectrum of the methyl bromide molecule. The $2e^{-1}$ (2E) state is split into two components by spin-orbit interaction. The $1e^{-1}$ (2E) state shows a Jahn-Teller splitting of 0.8 eV. In the insert the energy level diagram illustrating photoelectron transitions to states split by Jahn-Teller interaction.

5.3 Rotational fine structure

Rotational fine structure is normally not resolved in photoelectron spectra. At a resolution of about 10 meV, the line profiles may be influenced by the rotational excitations, but the individual lines cannot be seen. At a resolution below about 5 meV, which can be achieved with modern PES spectrometers, these influences become more clear and can sometimes be used to draw conclusions about the molecular geometry and the intensity of different rotational branches. For diatomic molecules, and larger molecules containing hydrogen, like H_2O or HF , for which the spacings between the individual components of the rotational structure are comparatively large, it may even be possible to observe this fine structure.

Figure 19 shows, as an example, a recording of the outermost line in the photoelectron spectrum of the HF molecule at a resolution of about 3-4 meV and with 18 eV photon energy. In this case, two spin-orbit split states are present which lead to a rather complicated line structure. Experimental (solid line) and calculated (broken line) spectrum of HF showing transitions to the $X^2\Pi$ ($v=0$) ionic

state are shown in the figure. The bar diagrams indicate various rotational transitions. The designations 1 and 2 refer to the $^2\Pi_{3/2}$ and $^2\Pi_{1/2}$ spin-orbit split components, respectively.

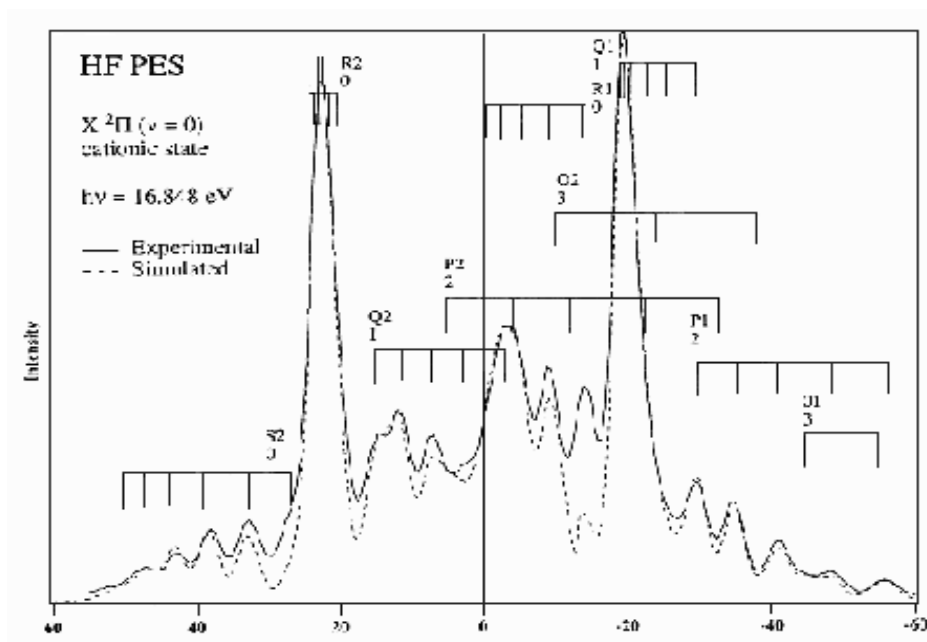


Fig.19. Experimental (solid line) and calculated (broken line) spectrum of HF showing transitions to the X 2Π ($v=0$) ionic state. The bar diagrams indicate various rotational transitions. The designations 1 and 2 refer to the $2\Pi_{3/2}$ and $2\Pi_{1/2}$ states, respectively.

6. PHOTOELECTRON ANGULAR DISTRIBUTIONS

Till now we have been dealing only with energy distribution of the photoelectron probability current, but the cross section (9) implies that a distribution in space (ejection angles) exist as well. We shall discuss this aspect of photoemission having in mind that it has a twofold relevance. On the one side angular distribution of photoelectrons is relevant to highlight fine details of photoionization dynamics (hence they are a stringent test for quantum description of radiation

matter interaction). On the other side accurate description of this phenomenon provides the basis for various spectroscopies based on diffraction of the photoelectron from surroundings atoms that are aimed at studying local geometrical order in molecules, clusters and solids [9].

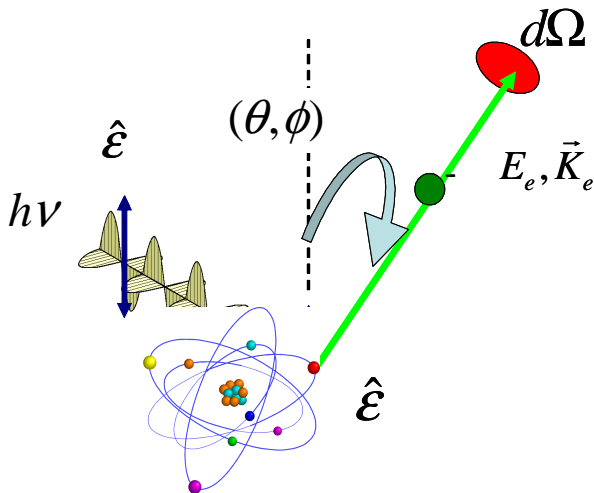


Figure 20. Schematics of an angle resolved photoemission experiment. The linearly polarized light $h\nu$ photoionises an electron with kinetic energy E_e within the solid angle $d\Omega$ in direction (θ, ϕ) with respect to the electric polarization vector $\hat{\epsilon}$.

Let's start from the simple atomic case. Starting from equation (9), it can be shown that, for linearly polarized light and for transition to a well defined ionic state (for fixed photon and photoelectron energies that satisfy the energy conservation δ function), the photoemission cross section reads:

$$\frac{d\sigma}{d\Omega} \propto \frac{1}{h\nu} \sum_{A,B} \left| \hat{\epsilon} \cdot \langle \epsilon_l | \vec{r}_j | \phi_j(\vec{r}_j, \sigma_j) \rangle \langle \Psi_B^{(N-1)} | \Psi_R^{(N-1)} \rangle \right|^2 \quad (12)$$

Hence, we expect the photoelectron current to depend upon direction under which the photoelectron is detected, with respect to polarization vector (see figure 20), and characteristics of the single particle orbitals involved, both bound and continuum.

All molecular and atomic orbitals have a characteristic angular distribution of electrons. This means that the intensity of all final states that we measure in a spectrum will have a certain angular dependence. Upon validity of the approximations of expression (9), the angular distribution of the emitted photoelectrons can be described using one single parameter, the asymmetry parameter β . In practice it means that the photoelectron distribution is symmetrically distributed about the polarization direction. Furthermore, upon dipole approximation the photoelectron will be ejected with a continuum wavefunction with $\ell = \pm 1$ with respect to the single particle hole quantum state left behind (this is because the incoming photon carries an unitary angular momentum). This gives an angular distribution of the ejected electron that obeys the relation:

$$\frac{d\sigma}{d\Omega} \propto \frac{\sigma}{4\pi} [1 + \beta P_2 \cos(\vartheta)] \quad (13)$$

where β spans from -1 to 2 . Expected angular dependence of the atomic photoelectron current for selected β values are reported in figure 21.

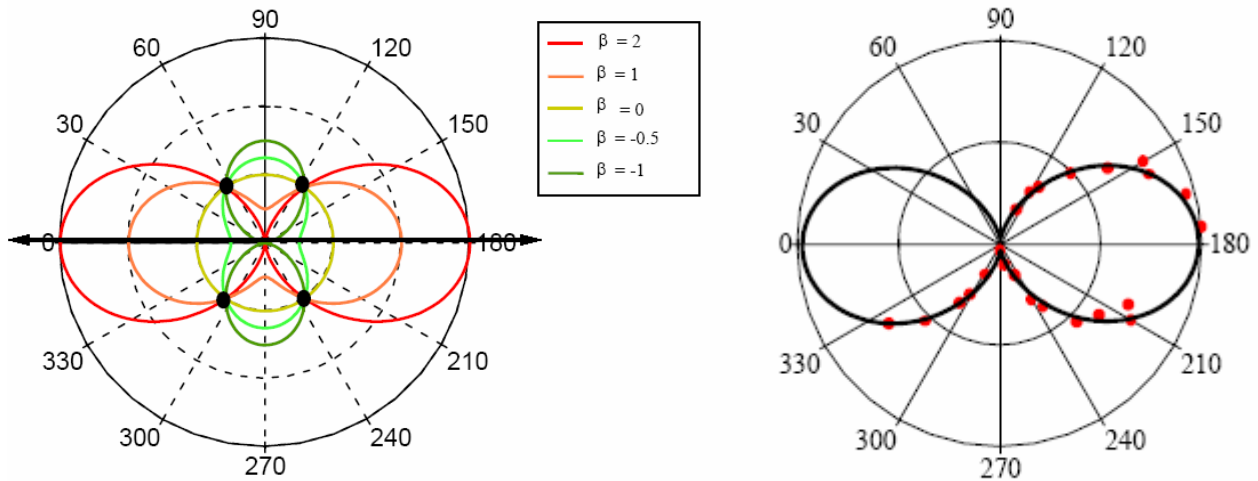


Figure 21. *Angular distribution of photoionisation in polar co-ordinates experimental (right panel) and calculated according to (13) for different values of β . The polarisation vector ϵ is reported as a black bold arrow. Magic angle has been indicated by a black point. Experimental results are relative to He and the best fit to the data is obtained for $\beta=2$.*

By studying this figure it can be seen that there are four places at which photocurrents are expected to be independent from β values. This occurs at the so-called magic angle of 54.74° . At this angle the photocurrent only depends on the total cross section σ and not on the light polarization or the angular momenta of the photoelectron wavefunction or the symmetry of the initial state. That this description is mostly correct in the case of isolated atoms is demonstrated by the good agreement between experimental results on He (red dots) and the theoretical prediction for $\beta=2$ (full line) shown in the right panel of figure 21.

What happens to photoelectron angular distributions when the atom from which the photoelectron is generated is surrounded by neighboring ones (i.e. in molecules cluster and solids)? The photoelectron wavefunction gets scattered from each individual atom and the photoelectron analyzer collects a photoelectron current that is a coherent superposition of source photoelectron wavefunction and point scattered wavefunctions, as schematically shown in figure 22.

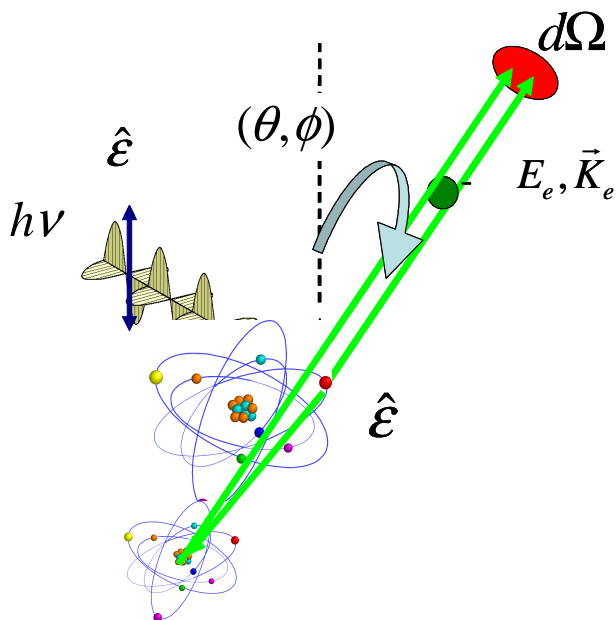


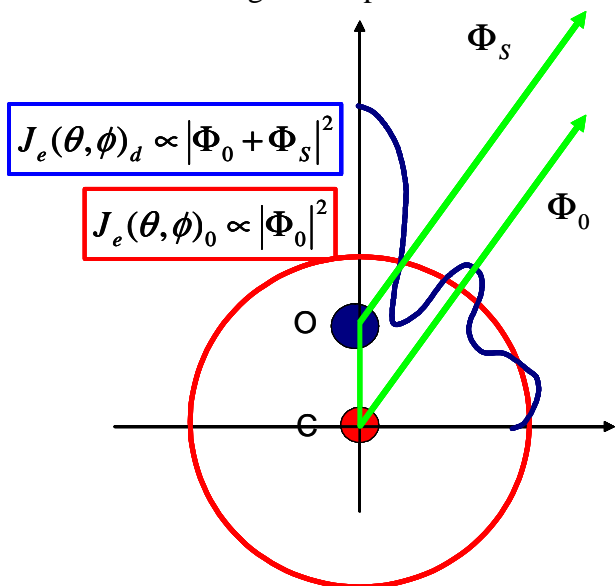
Figure 22. Schematics of an angle resolved photoemission experiment from a dimmer oriented in space. The linearly polarized light $h\nu$ photoionises an electron with kinetic energy E_e . The photoelectron current detected within the solid angle $d\Omega$, in direction (θ, ϕ) with respect to the electric polarization vector $\hat{\epsilon}$, is determined by coherent superposition of wavefunctions directly generated by the photoemission process and elastically diffused by the neighbor atom.

The angular distribution is not any more a smooth distribution determined by β , it will show two main features: a forward intense peak along atom-atom direction, and a diffraction pattern at

all other scattering angles. It can be shown that while in the case of an isolated atoms the measured photoelectron current is proportional to the square modulus of the unperturbed photoelectron wave function, i.e. $J_e \propto |\Phi_0|^2$, in the presence of a scatterer it becomes proportional to the modulus square of the coherent sum of the unperturbed and scattered photoelectron wavefunctions, i.e.

$J_e \propto |\Phi_0 + \Phi_s|^2$. If we perform measurement of the angular distribution of the photoelectrons

ejected from a fixed in space molecule, what is observed is schematically shown in figure 23 for the case of an aligned in space CO diatomic molecule.



Assuming that a core photoelectron is ejected from the carbon atom, the red line represent the polar probability distribution determined by the unperturbed wavefunction, while the blue one represents modulation introduced in the photoelectron angular distribution by interference of the direct and scattered wavefunctions. The intense forward lobe aligned with the molecular axis is to be interpreted as the 0th order peak of the angular diffraction pattern. Intensity maxima appearing at larger angles are higher order diffraction peaks.

Figure 23. Pictorial view of the photoelectron angular distribution for C1s ionization of an aligned in space CO molecule.

It is a crucial issue to establish validity for this simple scheme of interpretation of the photoelectron angular distributions, particularly in the case of core ionization, as it will constitute the cornerstone for applications to solids and surfaces, i.e. for the so-called *photoelectron diffraction*.

Modern experimental methods allow to align in space molecules either by attaching them to surfaces or by determining ex-post direction of the molecular axis. The latter method is more

complex as it requires to measure, coincident in time, distribution of both photoelectrons and molecular ions; but it allows to study free molecules and constitute a stringent test for the aforementioned model. Forward scattering and diffraction features are clearly seen in the experiment performed on aligned in space CO molecule and reported in figure 24. The photon energy was 321 eV and photoelectrons angular distribution was measured in two modes: with the molecular axis parallel (a) or perpendicular (b) to the light electric vector \vec{E} .

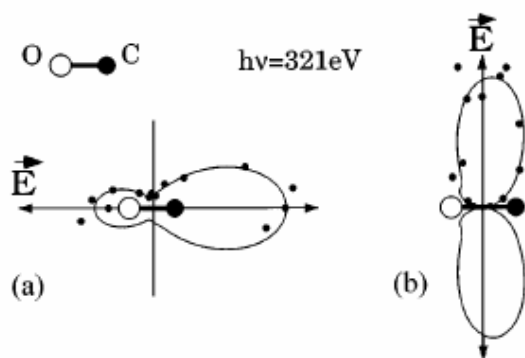


Figure 24. *1s* photoelectron angular distributions for an aligned in space CO molecule. The two results are relative to orientation of the molecular axis parallel (a) or perpendicular (b) to the light electric polarization vector.

Dipole selection rules impose an angular momentum $l=1$ to the $1s$ photoelectron wavefunction Φ_0 . Hence, according to equation (13), the isolated atom angular distribution is a cosine-like function with the two maxima pointing along the \vec{E} axis. In the molecular case (a), the angular distribution is dominated by the forward 0^{th} order diffraction peak as the intensity of the unperturbed wavefunction is low away from the molecular axis. In the (b) case Φ_0 is weak along the molecular axis while has maxima perpendicular to it, hence the photoelectron angular distribution is dominated by higher order diffraction peaks. These findings have been confirmed by several other independent experiments on similar or different molecular target, thus providing a sound background for validity of the aforementioned photoelectron diffraction model.

7. HOLE STATE RELAXATION

We have seen that the main peculiarity of photoemission peaks is the linear dispersion of their characteristic kinetic energy with the photon energy (see equation 3). Inspecting whichever full energy distribution of photoelectron current, we discover that, besides photoemission peaks, it displays further peaks whose energy is characteristic of the sample but does not change by changing the photon energy. Origin of these peaks can be explained in a elementary way by the energy diagram shown in figure 25.

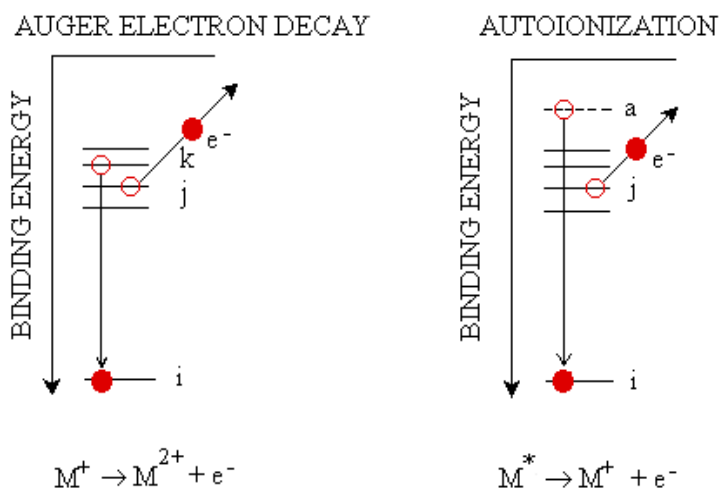


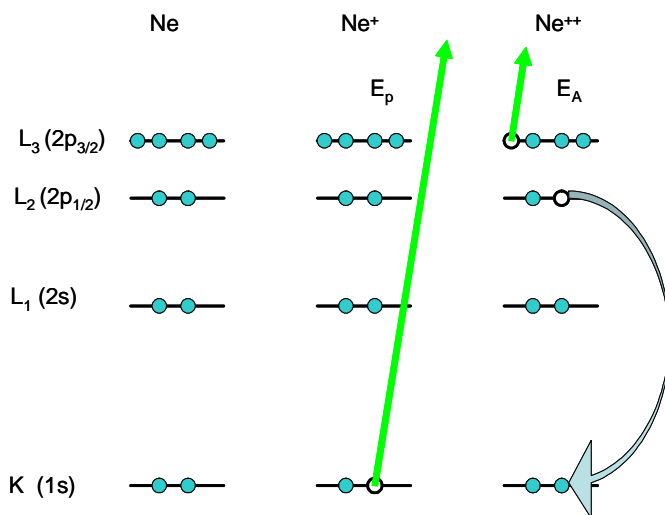
Figure 25. Schematics of the secondary processes leading to electron emission by the decay of a highly excited ionic or neutral system. Usually, the Auger process is associated with the decay of a cation whereas the decay of a neutral system is referred to as autoionization. Using synchrotron radiation it is possible to resonantly

populate highly excited states of the neutral system.

The core hole state $|i\rangle$ is created either by direct photoemission (panel a) or by excitation to the excited state $|a\rangle$. Obviously, the first process is always possible provided the photon energy exceeds the ionization threshold, while the second (panel b) only when the photon matches the difference in energy between state $|i\rangle$ and $|a\rangle$. In both cases, the $|i\rangle$ hole state is part of a singly ionized/neutral excited state whose lifetime is finite. This state will decay through electron-electron interaction within the target either in a radiative way (fluorescence) or in a non radiative way i.e. ejecting an electron in the continuum (autoionization). This latter decay channel is dominant for low Z atoms and is usually termed as autoionization or Auger according to the charge state of the final ion, single or double respectively. It is evident that the energy spectrum of the autoionizing electrons will reflect the target energy structure through the difference between energy of the final and initial states in as much as the energy of the Auger/autoionization transition matches the separation energy between $|i\rangle$ and $|a\rangle$.

7.1 The Auger decay

Auger electrons emission is usually described within a two step approximation in which decay incoherently follows the core hole creation $h\nu + A \rightarrow A^+ + e_p \rightarrow A^{++} + e_p + e_A$. The energy distribution of the Auger electrons (e_A) is independent from the photon and photoelectron (e_p) energies, it will be determined by the difference in energy between the intermediate singly ionized state and the final doubly ionized state $E_{Auger} = E_{A^+} - E_{A^{++}}$. Hence, the Auger energy spectrum will be formed by groups of line transitions, one for each core hole state, having as many components as the multiplet configurations allowed for the double hole final state. It is therefore spontaneous to indicate each Auger transition with a three letters label. The first letter refers to the orbital involved in the intermediate core hole state creation, the other two to the orbitals that generate the doubly ionized final state. Let's take the Ne atom as an example. In its ground state configuration the shells K (n=1) and L (n=2) are fully occupied (see leftmost panel in figure 26). According to this convention, the Auger transition depicted in the rightmost panel of figure 26 is KL_2L_3 . This is not the only possible Auger transition for the K core hole to decay, the main groups of transitions with their multiplet structures are listed in the following table.



ionized final state. Let's take the Ne atom as an example. In its ground state configuration the shells K (n=1) and L (n=2) are fully occupied (see leftmost panel in figure 26). According to this convention, the Auger transition depicted in the rightmost panel of figure 26 is KL_2L_3 . This is not the only possible Auger transition for the K core hole to decay, the main groups of transitions with their multiplet structures are listed in the following table.

Figure 26. Schematics of the KL_2L_3 Auger process in Ne. E_p and E_A are kinetic energy of the photoelectron and Auger electron, respectively.

Auger Transition	Double ion valence configuration	Multiplet Terms
KL_1L_1	$2s^0 2p^6$	1S_0
$KL_1L_{2,3}$	$2s^1 2p^5$	$^1P_1, ^3P_0, ^3P_2, ^3P_1$
$KL_{2,3}L_{2,3}$	$2s^2 2p^4$	$^1S_0, ^3P_0, ^3P_2, ^1D_2$

The simplest, though coarse, way to calculate individual Auger transition energies is within a simple one-electron model, i.e. ignoring relaxation and final state effects. Within this approximation the multiplet splitting is ignored and the Auger energy can be deduced from the binding energy of the individual orbitals, for instance:

$$E_A(KL_1L_2) = E(K) - E(L_1) - E(L_2, L_1) \quad (14)$$

where the latter energy is the binding energy of the L_2 orbital computed in presence of a hole in L_1 . There are several methods to calculate more accurately, even ab-initio, Auger transition energies but to describe them is beyond the scope of this lecture. The simplified scheme so far outlined is sufficient for interpreting an atomic Auger spectrum such as the one displayed in figure 27.

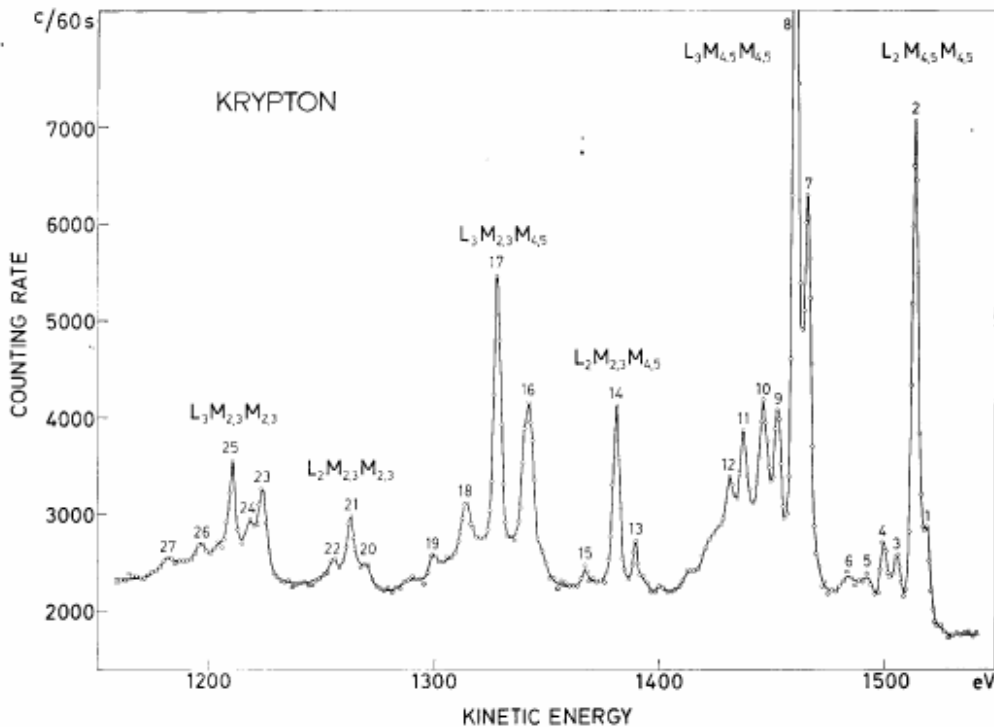


Figure 27
 Auger spectrum
 of gaseous
 Krypton. The
 energy
 distribution is
 recorded as a
 function of the
 Auger kinetic
 energy. The
 principal Auger
 lines are indexed
 according to the
 usual notation
 (see text).

It shows the energy distribution of Auger ($N(E_A)$) electrons from gaseous Krypton as a function of their kinetic energy. The principal transitions can be readily assigned through relation (14) and are indexed according to the aforementioned notation. Multiplet splitting of each individual principal transition is also evident. This effect is better seen in the blow-up of the free Zn atom $L_3M_{4,5}M_{4,5}$ spectrum of figure 28. In Zn, all shells from K to M and the 4s subshell are full, hence a simple two-particles (i.e. two holes in the final doubly ionized state) multiplet structure is appropriate to describe its Auger spectrum. The appropriate spectroscopic terms are: 1S_0 , 1G_4 , $^3P_{0,1,2}$, 1D_2 , $^3F_{2,3,4}$. All of these spectroscopic terms are clearly recognized in the spectrum of figure 28 with the 1G_4 being the dominant one. The experimental result is compared with predicted Auger transitions, shown in the figure with bars whose height is proportional to the relative intensity. The overall agreement between theory and experiment is rather good, thus demonstrating that, in spite of the complexity, most features of Auger spectra can be predicted and calculated, thus providing a powerful tool for studying correlated behavior of matter as the final state is always a two interacting particle one. Naturally, such a detailed description of the Auger spectrum is obtained with a model that goes beyond the simple one summarized by equation (14) and that account for spin-orbit coupling, relaxation of the ionic states, final state effects and hole-hole correlation energy. For what concerns intensity of the transitions, the two-step model can be invoked to allow us to compute the probability of an Auger transition as the product of those relative to the core all

creation and decay separately. Hence the probability for an Auger transition initiated by a photon that ionizes a system in state $|0\rangle$ to a core hole state $|i\rangle$ that eventually decays to the doubly ionized state $|f\rangle$ is:

$$P(0,i,f) \propto \left| \langle f \varepsilon_p \varepsilon_A | C | i \varepsilon_p \rangle \right|^2 * \left| \langle i \varepsilon_p | D | 0 \rangle \right|^2 \quad (15)$$

Where C and D are coulomb and dipole operators, respectively. The two step model is appropriate as long as the core hole lifetime is much longer than coulomb interaction time. On the contrary, the single step model is do be adopted. In this frame the core hole state is an intermediate state for the second order transition that leads to the doubly ionized system and the probability reads:

$$P(0,i,f) \propto \left| \int \frac{\langle f \varepsilon_p \varepsilon_A | C | i \tau \rangle * \langle i \tau | D | 0 \rangle}{E_A + E_p - E_\tau - h\nu - i\Gamma/2} d\tau \right|^2 \quad (16)$$

Where τ are virtual intermediate states and Γ is the core hole lifetime broadening. It is therefore evident that the main driving force behind Auger transition is the coulomb interaction among bound electrons of the system. Furthermore, through the final state $|f\rangle$ correlated properties of the system influence the Auger cross-section.

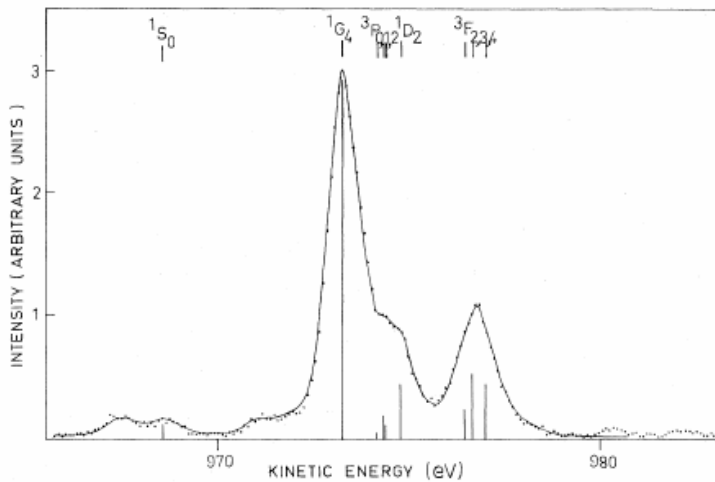
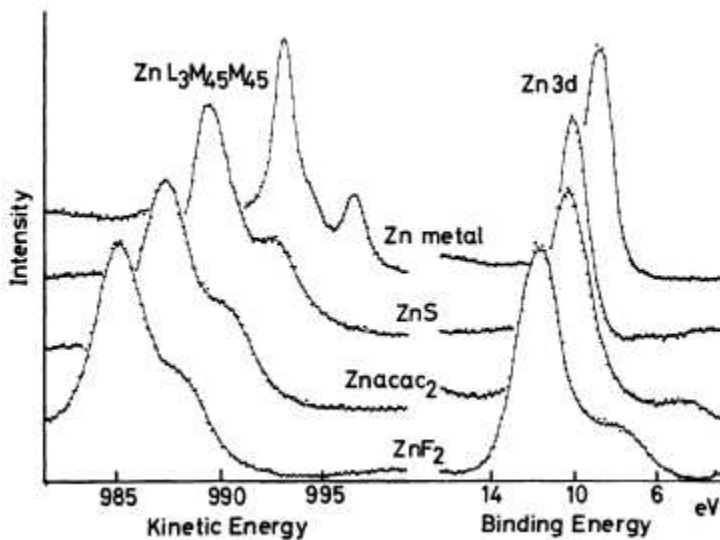


Figure 28. *The free Zn atom $L_3M_{4,5}M_{4,5}$ spectrum. . The energy distribution is recorded as a function of the Auger kinetic energy. Relevant spectroscopic terms are shown on the top part. Bars are located at the calculated transition energies, the height is proportional to the relative intensity.*

Similarly to what discussed for core photoemission, also Auger spectra are sensitive to the local chemical environment. This effect is clearly shown in figure 29 where the Zn $L_3M_{4,5}M_{4,5}$ is shown together with the Zn 3d photoemission spectrum for a few zinc compounds. We first observe that



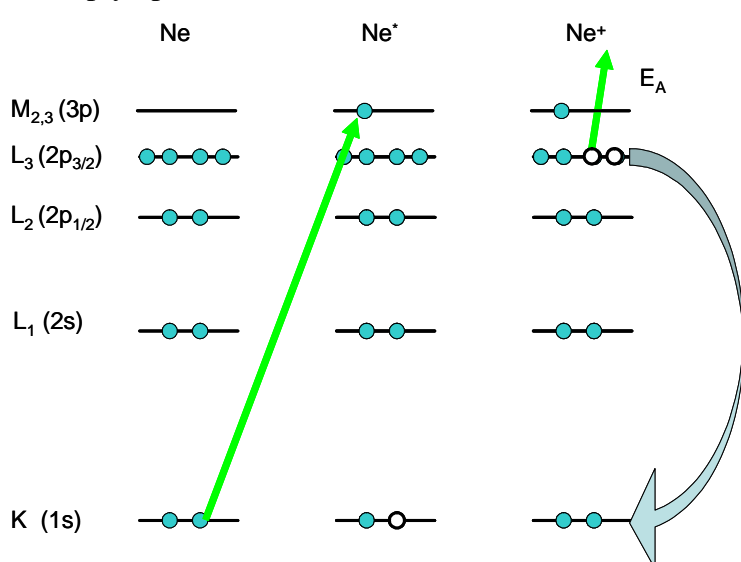
the zinc metal Auger spectrum preserves most of the multiplet structure of the free atom, as it is for many highly correlated systems. The 1G_4 component (the highest peak) is shifted by almost 7eV in going from Zn metal to ZnF₂, a chemical shift even larger of the one suffered by the 3d photoemission peak.

Figure 29. *The $L_3M_{4,5}M_{4,5}$ spectra of Zn in different compounds display chemical shifts of amplitude comparable to the one of the Zn 3d photoemission peak.*

To finish with analyzing Auger spectroscopy sensitivity to local matrix properties it is to be mentioned that Auger electrons angular distributions display diffraction patterns of the same sort of those displayed by core photoelectrons. Hence, Auger spectroscopy is suitable to study local spatial and electronic properties in molecules, clusters and solids. Interpretation of Auger spectra is less straightforward than photoemission one as the final state of the former is doubly instead of singly charged as it is in the latter. In conclusion, in spite of its inherent interpretation difficulties Auger spectroscopy is an excellent tool to study local electron correlation properties in the various states of aggregation.

7.2 Resonant Auger and photoemission

So far we have discussed core hole de-excitations having a singly charged ion as initial state for the Auger decay. Let's now consider the case depicted in the rightmost panel of figure 25, i.e. the autoionization of a core excited system. In X-ray absorption language we are interested in describing the decay channels of the near absorption edge resonances (XANES). This is an autoionization process that ends in a singly ionized state, which is a state identical to the one reached by a direct photoionization. Let's again take Ne as an example. As shown in the schematics of figure 30, by absorbing a photon of appropriate energy the 1s electron is promoted to the empty 3p level. Afterwards, the core excited Ne* autoionizes filling up the core hole and ejecting a valence (2p in the example).



ejecting a valence (2p in the example) Electron. This process is usually termed as a spectator (the 3p state) Auger decay and the final state, which is identical to the final state of a transition satellite to the 2p_{3/2} photoionisation, is termed as a 1particle 2hole state.

Figure 30. Schematics of the resonant Auger process in Ne. the 1s electron is promoted to the empty 3p level. The core excited Ne* autoionises by filling up the core hole and ejecting a valence electron(2p_{3/2})

In other words, the final ionic state depicted in figure 30 can be created either by a resonant spectator Auger decay or by direct photoionization.

What does it happens when the energies of the resonant Auger and the photoelectron coincide? We shall discuss it by the help of a specific result obtained for an Ar atom. In figure 30a are sketched the lowest ionic states of argon, that are single hole (1h) states, 3p⁻¹ or 3s⁻¹. At higher energies a multitude of 2h1p states, belonging to the 3p⁻²nl, 3p⁻¹3s⁻¹nl, or 3s⁻²nl manifolds, are found. In direct, nonresonant photoemission, the 1h states are strongly dominant, and the 2h1p states are observed as weak satellites. The photoemission spectra of the reactions $h\nu + Ar \rightarrow Ar^+(3s,3p)^{-2}nl + e^-$ was recorded for several different photon energies across the resonance $h\nu + Ar \rightarrow Ar^*(2p_{3/2}^{-1}4s)$ (see left part of figure 30 panel a). Photoemission spectra as measured for different detunings Ω are shown in panel B of figure 30. Let's focus on the peak indexed B, it correspond to the unresolved transitions $h\nu + Ar \rightarrow Ar^+(3p)^{-2}5s,4f + e^-$ is almost absent when the photon is tuned out of resonance ($\Omega= 7.5\text{eV}$) become dominant when tuning the photon on resonance ($\Omega= 0\text{eV}$). It is therefore evident that for selected photoionisation channels the resonant excitation is dominant over the direct ionisation one. Indeed, panel c of figure 31 shows that tuning the photon energy across

the core resonance the photoionisation cross section rises by almost an order of magnitude reaching its maximum for on tuning condition. Observing the behaviour as a function of Ω of the transition $h\nu + Ar \rightarrow Ar^+ (3p)^{-2}3d + e^-$, we notice that the cross section on tuning is larger than off tuning, but the lineshape is highly asymmetric with respect to the resonance energy, as it is the case for all the other photoemission investigated and reported in figure 31c. The origin of this asymmetry is in the double quantum path that, for a given photon energy, can be followed in going from the ground neutral state to the singly ionised 2h 1p states. The final ionic state is created following the resonant or the direct channel with an identical wavefunction but with a different phase. Upon changing the detuning, the phase associate with the direct channel changes slowly and monotonically, while the resonant channel one changes rapidly. As long as amplitude of one channel is much larger than the other, the ionisation cross section reduces to the direct photoemission (equation 12) or to the resonant Auger one (equation 16).

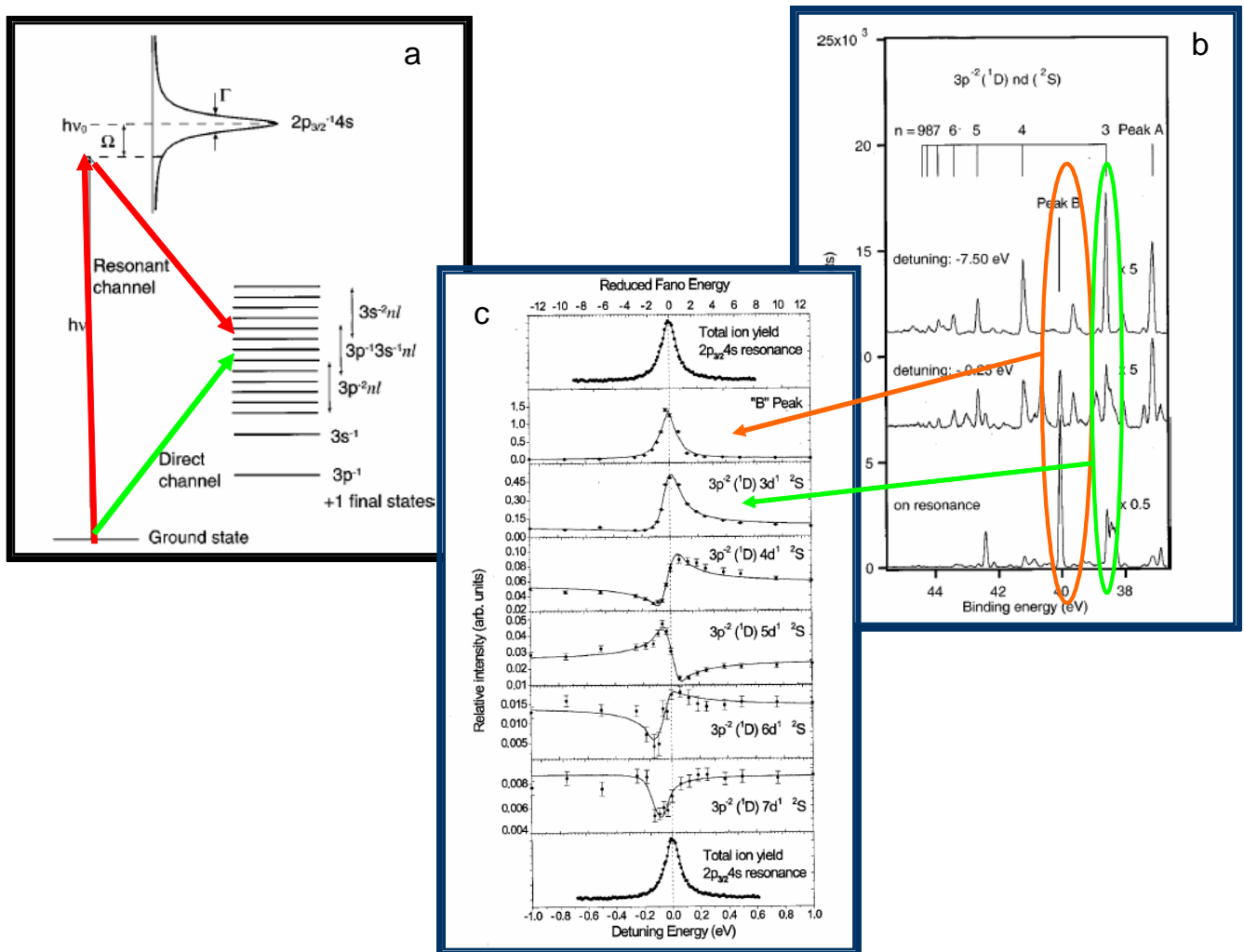


Figure 31. Schematics of the resonant Auger process in Ar. The 2p electron is promoted to the empty 4s level. The core excited Ar* autoionises by filling up the core hole and ejecting a valence electron(3p). See text for details.

When amplitude of the matrix element of the two competing channels becomes comparable they should be coherently added and the probability of the process becomes:

$$P(0, i, f) = \left| \int \frac{\langle f \mathcal{E}_A | C | i \tau \rangle^* \langle i \tau | D | 0 \rangle}{E_A + E_p - E_\tau - h\nu - i\Gamma/2} d\tau + \langle f \mathcal{E}_A | D | 0 \rangle \right|^2 \quad (17)$$

Probability of the resonant Auger\photoelectron process is therefore modulated by the interference term resulting from squaring the sum of the two amplitudes. Upon rapid change of the resonant channel phase, interference rapidly switches from constructive to destructive, thus yielding the peculiar lineshapes (Fano profiles) displayed in panel 31c. It can be readily verified that if one of the two amplitudes becomes negligible equation 17 reduces to equation 16 or 12.

In summary, resonant Auger\photoelectron provides:

- a. an effective spectroscopy of many-electron excited states that are otherwise inaccessible to conventional electron spectroscopies
- b. An unique way to highlight phase changes in the final state wavefunction that are just not detected by other spectroscopies

NOTES

[Note 1] The Franck-Condon Principle

Optical transitions have a vibratory fine structure that is usually not resolved and leads to broad featureless bands that are typically non-symmetric.

Optical transitions occur between wavefunctions that have vibratory and rotatory contributions (sub-levels).

As discussed previously, only the vibratory ground state is populated in most bonds. This means that our optical transitions will occur from the n=0 vibratory level.

For the excited state, the situation is slightly more complex. As was first pointed out by Franck and Condon, optical transitions are "vertical", which means, that they occur so rapidly (10^{-15} sec), that the framework of nuclear coordinates cannot follow. All internuclear distances and angles (including those involving the solvent cage or different conformations) are therefore preserved in the excited state. This means, that the energies of vibrational and rotational transitions do not change during the optical transition.

They will change after the optical transition, because the nuclei adjust their position to minimize the total energy of the new electron configuration.

REFERENCES

- [1] C.S. Fadley “Basic Concepts of X-ray Photoelectron Spectroscopy”, in Electron Spectroscopy, theory, techniques and applications, Brundle and Baker Eds. (Pergamon Press, 1978) Vol. 11, ch.1 available at: [HTTP://WWW.PHYSICS.UCDAVIS.EDU/FADLEYGROUP](http://www.physics.ucdavis.edu/fadleygroup)
- [2] S. Mobilio and A. Balerna in “Synchrotron Radiation Fundamental Methodologies and Applications (SIF Conference Proceedings vol 82, pg. 1)
- [3] G. Margaritondo, Y. Hwu, G. Tromba in “Synchrotron Radiation Fundamental Methodologies and Applications (SIF Conference Proceedings vol 82, pg. 25)
- [4] S. Hufner “Photoelectron Spectroscopy, principle and applications” (Berlin Springer 2003) 3rd Edition
- [5] C.M. Bertoni in “Synchrotron Radiation Fundamental Methodologies and Applications (SIF Conference Proceedings vol 82, pg. 95)
- [6] J. H. Moore, C.C. Davis, M.A. Coplan “Building Scientific Apparatus” Perseus Books, Reading, Massachusetts Chapter 5
- [7] V. Schmidt “Photoionization of atoms using synchrotron radiation” Report on Progress in Physics 55(1992)1482
- [8] C. Mariani in “Synchrotron Radiation Fundamental Methodologies and Applications (SIF Conference Proceedings vol 82, pg. 211)
- [9] G. Paolucci “Photoemission from solids”, this school